SUBDUCTION INITIATION OF THE NEO-TETHYS OCEAN IN CENTRAL IRAN BASED ON U-PB GEOCHRONOLOGY, GEOCHEMICAL AND ND ISOTOPE DATA OF THE ASHIN OPHIOLITE

Nargess Shirdashtzadeh*,✉, Harald Furnes, Nathaniel R. Miller***, Elton Luiz Dantas°, Ghodrat Torabi*** and **Thomas C. Meisel°°**

* *Department of Geology, University of Isfahan, Iran.*
** *Department of Earth Science, University of Bergen, Norway.*
*** *Department of Geological Sciences, University of Texas at Austin, USA.*
° *Institute of Geosciences University of Brasilia, Brazil.*
°° *General and Analytical Chemistry, Montanuniversität, Leoben, Austria.*
✉ *Corresponding author, e-mail: nshirdasht@gmail.com*

Keywords: *subduction initiation; Ashin Ophiolite; Neo-Tethys Ocean; Iran*

ABSTRACT

Subduction initiation (SI) ophiolites are critical for reconstructing plate tectonic and magmatic evolution along ancient convergent margins. Here we integrate clinopyroxene and whole rock chemical compositions, whole rock Nd isotopic compositions, and zircon U-Pb geochronology to demonstrate that the Ashin ophiolite between the Torbat-e-Heydarieh-Sabzevar and Nain-Baft ophiolitic Belts, records the initiation of late Early Cretaceous subduction magmatism and formation of Neo-Tethys oceanic crust. Clinopyroxene and whole rock geochemical compositions of Ashin non-metamorphosed pillow lavas and ortho-amphibolites (metamorphosed pillow lavas) and ortho-amphibolitic dikes (metamorphosed diabase dikes) and whole rock compositions of comparable ophiolite exposures from Nain, Dehshir, and Shahr-Babak areas support a basaltic protolith generated during a subduction initiation system. Based on geochemical data, Sm/Nd > 0.4, Lu/Hf > 0.3, $Ce_N/Yb_N < 1.2$, $Dy_N/Yb_N < 1.2$, $Gd_N/Yb_N < 1$, $La_N/Yb_N < 1$, Th/Nb < 0.2 ratios, and $\varepsilon Nd_I > +9$ can characterize the forearc basalt (FAB) affinity of ophiolitic mafic rocks. Geochronological (~ 107-94 Ma radiolarian cherts) and geochemical characteristics of the Ashin pillow lavas reflect a MORB-like forearc basin formed during subduction initiation towards the end of the Early Cretaceous. Then a younger group of basic pillow lavas and dikes formed and metamorphosed (to the amphibolites and amphibolitic dikes) in MORB-like (before 104 Ma) to SSZ-like (~ 97 Ma) SI settings based on zircon U-Pb ages and geochemical data. This short-lived oceanic basin (~ 13 Myrs, from ~ 107 to 94 Ma) closed at around 60 Ma (in Paleocene).

INTRODUCTION

An extended characterization and classification of ophiolites, compared to that of the original Penrose classification of 1972 was presented in Dilek and Furnes (2011; 2014). In the latter classification, ophiolites are defined as "suites of temporally and spatially associated ultramafic to felsic rocks evolved from separate melting episodes and processes of magmatic differentiation in particular oceanic environments". Based on various combinations of immobile trace elements (e.g., Pearce, 2014; Saccani, 2015), combined with their architecture, the ophiolites can be subdivided into two main categories and several subgroups. The two main categories are based on whether subduction - controlled fluid and melt production contributed to their magmatic evolution: (1) subduction-unrelated, and (2) subduction-related ophiolites (e.g., Furnes and Dilek, 2022). Subduction-unrelated ophiolites include Mid-Ocean-Ridge (MOR), Rift (R), Continental Margin (CM), and Plume (P) types. The subduction-related category includes Backarc (BA), Forearc (FA), Backarc to Forearc (BA-FA) and Volcanic Arc (VA) types (e.g., Dilek and Furnes, 2014; Furnes and Dilek, 2017; Furnes et al., 2020), depending on the extent of the subducting slab influence in melt formation.

It is widely accepted that global plate motions are mostly powered by the sinking of negatively buoyant oceanic lithosphere in subduction zones (e.g., Becker and Faccenna, 2011; Lu et al., 2015; Stern and Gerya, 2018). Subduction initiation (SI) ophiolites (forearc ophiolites) are therefore critical clues for reconstructing plate tectonic and magmatic evolution along ancient convergent margins. Based on studies of the modern Izu-Bonin-Mariana (IBM) forearc magmatic rocks, Reagan et al. (2010) proposed that most 'Tethyan ophiolites' are exhumed forearc lithosphere above a new subduction zone (so-called suprasubduction zone or SSZ), chemically ranging from MORB (mid-ocean ridge basalt)-like forearc rocks during early subduction initiation (SI) to subsequently become SSZ-like forearc lithologies. Stern et al. (2012) suggested that subduction-related forearc oceanic lithosphere is relatively easy to emplace on continental crust to form ophiolites, compared to more difficult emplacement of subduction-related backarc oceanic lithosphere, and almost impossible emplacement of the 'subduction-unrelated' MORB crust formed in true mid-oceanic ridges. Reagan et al. (2010) suggested that forearc basalts (FAB) from the IBM arc system, as the first products of subduction initiation, either formed by processes that differ from normal MORB or are derived from mantle that is more refractory than DMM (Depleted MORB source Mantle).

A recent study of Alpine-Himalayan orogenic belt (AHOB) ophiolites (Fig. 1a) has classified these Mesozoic subduction-related Tethyan ophiolites to dominantly backarc type (43%) rather than backarc-forearc (19%), forearc (8%), and volcanic arc (6%) types (Furnes et al., 2020). Eocene IBM forearc basalts (FAB) reflect a stronger prior depletion of their mantle source compared to the source of back-arc basin (BAB) and mid-ocean ridge basalts (MORB). Forearc basalts (FAB) are thought to be the first lavas to fill the space left by the sinking plate as subduction begins (Reagan et al., 2010). FABs have mid-ocean ridge basalt (MORB)-like

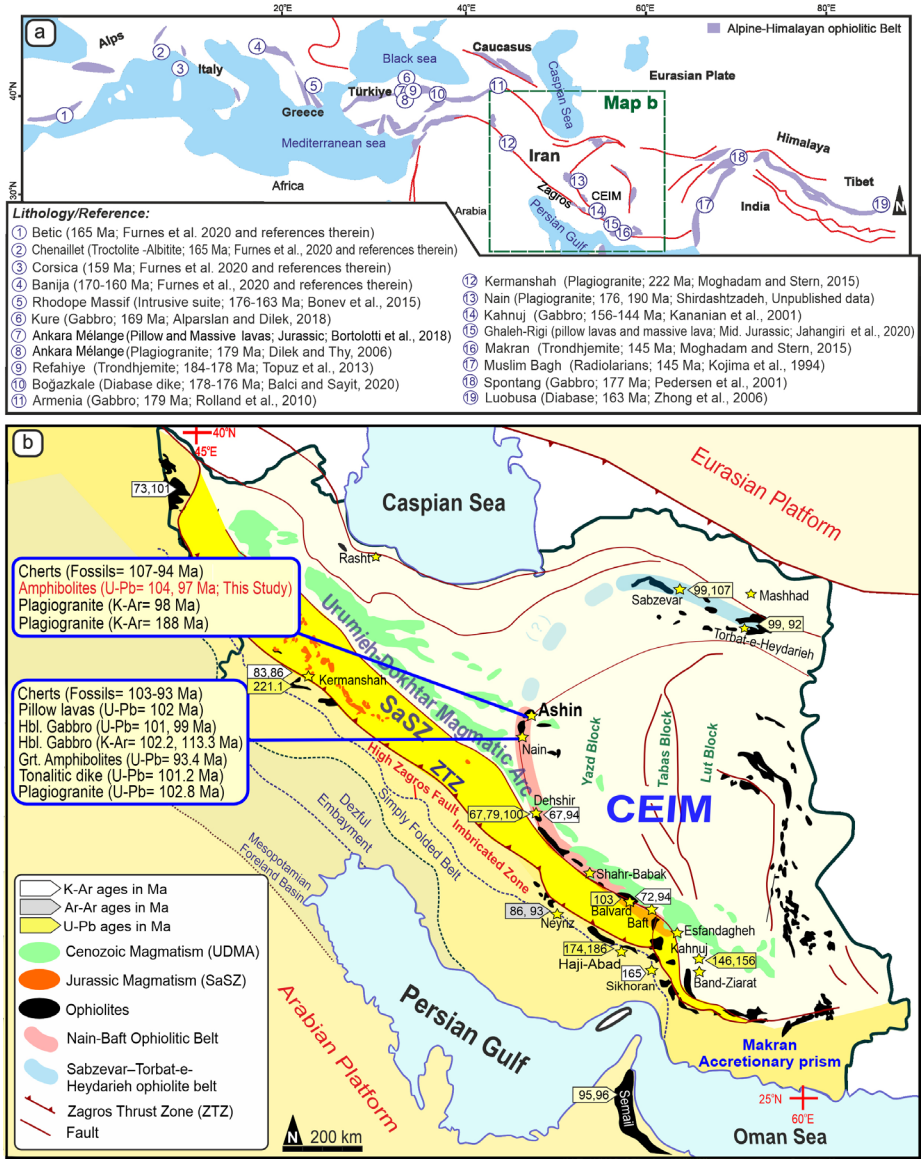

Fig. 1 - (a) Distribution of representative examples of Mesozoic SSZ-Type ophiolites of Alpine-Himalayan orogenic belt from the Alps to Turkey, Iran, India, and Tibet (Data from Table 1 in Furnes et al., 2020); (b) Simplified map of structural zones in Iran and distribution of the main Jurassic-Cretaceous ophiolites of Zagros Orogen (Khoy, Kermanshah, Neyriz, Haji-Abad, Esfandagheh, Nain, Dehshir, Shahr-Babak, Balvard, Baft, Kahnuj; Data and references from Table 1 in Moghadam and Stern, 2015) and Ashin (Sharkovski et al., 1984; Shirdashtzadeh et al., 2015; this study). CEIM= Central-East Ir;anian Microcontinent; SaSz = Sanandaj-Sirjan Zone).

compositions but differ from MORB by their lower high-field strength elements (TiO_2, P_2O_5, Zr), Ni, light rare earth element, and Ti/V, Zr/Y, Ce/Yb, and Zr/Sm relative to MORB (Shervais et al., 2019). Despite the apparently rare occurrence of AHOB Tethyan MORB-like forearc ophiolites (i.e., ~ 8%; Furnes et al., 2020), they can, however, if present, be used in determining the subduction initiation age. Time of subduction initiation and age of the slab's lithosphere are key constraints to reconstruct a given subduction zone (Yu et al., 2022).

Centrally positioned within the Alpine-Himalayan orogenic belt, Iran is of particular interest for its exposures of suprasubduction zone (SSZ-type) ophiolites, which facilitate reconstruction of the active Jurassic-Cretaceous Neo-Tethyan subduction margin (Fig. 1a-b). The oldest ophiolite exposures associated with subduction initiation occur around central Iran (including Sabzevar, Ashin-Nain, Dehshir, Shahr-Babak, Balvard, and Baft ophiolites; Fig. 1b). Ophiolites are situated within and along the margins of several tectonostratigraphic terranes (termed zones) that comprise the basement geology of Iran. These ophiolites were structurally emplaced in Paleocene time between the Sanandaj-Sirjan Zone and Central-East Iranian Microcontinent tectonostratigraphic terranes (e.g., Ghazi and Hassanipak, 2000; Moghadam et al., 2009; 2015; Shirdashtzadeh et al., 2010; 2014b; 2015; 2020; Omrani et al., 2013; Mattei et al., 2014; Pirnia et al., 2020) (Fig. 1b). Among them, the Ashin ophiolite is a poorly understood ophiolite-bearing mélange succession located on the northwest periphery of the Yazd Block (Fig. 1b). Previous geochemical and biostratigraphic studies proposed three possible Mesozoic SSZ tectonic settings for the Ashin ophiolite: 1) a Jurassic backarc for its amphibolite protolith (metamorphosed pillow lavas and basic dikes; Shirdashtzadeh et al., 2010; 2011; Torabi et al., 2011); 2) a Cretaceous forearc for unmetamorphosed sheeted dikes and pillow lavas (Sharkovski et al., 1984; Shirdashtzadeh et al., 2010; 2011; Torabi et al., 2011; Shirdashtzadeh et al., 2015; Pirnia et al., 2020); and 3), the hypothesis of broad upper plate extension associated with SI (Moghadam and Stern, 2021) would interpret Ashin ophiolite as related to SI, but in a backarc setting. In this contribution, we present new interpretations by providing new trace element and Nd isotopic compositions of mafic lavas and dikes from the Ashin ophiolitic mélange and minimum zircon U-Pb isotopic ages for non-metamorphosed pillow lavas, ortho-amphibolites and ortho-amphibolitic dikes. In general, clinopyroxene is relatively insensitive to disturbance by metamorphism and is another powerful petrogenetic

indicator, particularly for deciphering mafic rock origins (e.g., Yamasaki et al., 2006; Choi et al., 2008; Shirdashtzadeh et al., 2014a, 2014b; Khedr et al., 2014). Thus, we re-evaluate non-metamorphosed pillow lavas and amphibolites for trace element geochemistry of their clinopyroxene phenocrysts and clinopyroxene relicts, respectively. Here, we compare the whole rock composition data with those of typical backarc (BAB), intra-oceanic arc, and forearc basaltic (FAB) rocks of the modern IBM arc system (Izu, Bonin and Mariana data in GEOROC; http://georoc.mpch-mainz.gwdg.de) to assess analogous tectonomagmatic origins and likely settings within the Iranian sector of Neo-Tethyan convergent margin.

GEOLOGICAL SETTING

Neo-Tethyan ophiolitic complexes of the Alpine-Himalayan orogenic belt extend from Europe through Turkey, Iran, Oman, Pakistan, as far as Tibet (Fig. 1a). These ophiolites record Mesozoic magmatic and metamorphic evolution of the Neo-Tethys convergent margin on the southern margin of Eurasia and collision of continental fragments rifted from the northern margin of Gondwana (e.g., Stampfli and Borel, 2002; Dilek and Furnes, 2019). In the middle of the Alpine-Himalayan Orogen (Fig. 1a), Iran consists of Cadomian (~ 600-500 Ma) crust that was rifted from northern Gondwana and accreted to southern Eurasia in Permo-Triassic time (Stern et al., 2021). This crust was affected by extension-related magmatism in Jurassic time to form the Sanandaj-Sirjan Zone (SaSz), possibly associated with a passive continental margin. This passive margin collapsed in mid-Cretaceous time to form a new convergent margin and SI ophiolites, which spawned the igneous activity of the Urumieh-Dokhtar magmatic arc (UDMA) and the development of the accretionary complex of the Zagros Fold-and-Thrust Belt (Fig. 1b). Localities of the Ashin ophiolite sampled for the present study come from the Central-East Iranian Microcontinent zone (= CEIM; consisting of the Yazd, Tabas, and Lut blocks; Fig. 1b), a Cadomian terrane that is bounded by several Cretaceous SI ophiolites from Nain to Baft (including Ashin, Nain, Dehshir, Shahr Babak, Balvard, and Baft ophiolites; Fig. 1b), Sistan and Sabzevar (Agard et al., 2011; Wilmsen et al., 2015). Moghadam and Stern (2015) subdivided Iranian Neo-Tethyan ophiolites into 'Late Cretaceous' Zagros ophiolitic belts, Sabzevar-Torbat-e-Heydarieh, and Birjand-Nehbandan-Tchehel-Kureh, and 'Late Jurassic-Cretaceous' ophiolites (Makran). Paleomagnetic research suggests that the Neo-Tethys oceanic realm was characterized by Late Triassic-Jurassic spreading followed by Mid-Jurassic-Early Cretaceous rotation around the Central-East Iranian Microcontinent (Mattei et al., 2014, and references therein). These ages are in accord with the other Alpine-Himalayan orogenic belt ophiolites that contain ophiolitic Jurassic rocks (Fig. 1a).

Neo-Tethyan ophiolites in Central Iran

The Central East-Iranian Microcontinent (CEIM) in Central Iran is surrounded by Cretaceous ophiolites and ophiolitic mélanges of Ashin, Nain, Dehshir, Shahr-e-Babak, Balvard, and Baft ophiolites (so called "Nain-Baft Ophiolitic Belt") in the west and southwest, the Sabzevar and Torbat-e-Heydarieh ophiolites in the northeast (so called "Torbat-e-Heydarieh - Sabzevar Ophiolitic Belt"), the Sistan ophiolitic zone in the east (Fig. 1b). Despite of ambiguous and sometimes inconsistent conclusions, the island arc tholeiitic to MORB geochemical affinities of intermediate to mafic rocks generally indicate a forearc or backarc SSZ (suprasubduction) basin for these ophiolites (Moghadam et al., 2009; 2019b; Pirnia et al., 2020; Moghadam and Stern, 2021).

The Neo-Tethys oceanic basin along Torbat-e-Heydarieh - Sabzevar to Nain-Baft ophiolitic Belts, between Sanandaj-Sirjan Zone and Central-East Iranian Microcontinent, occurred by mantle uprising and generation of mantle peridotites, diabasic rocks, plagiogranites, and basaltic pillow rocks (e.g., Moghadam et al., 2009; Shirdashtzadeh et al., 2014a; 2020). Based on previous findings (e.g., Sharkovski et al., 1984; Kananian et al., 2001; Mattei et al., 2014), long-lived spreading of this oceanic basin occurred in Late Triassic-Early Jurassic time until closure from Late Cretaceous to Paleocene times with emplacement of Neo-Tethyan ophiolites onto Central-East Iranian Microcontinent continental basement (Torabi et al., 2011; Shirdashtzadeh et al., 2015; Pirnia et al., 2020 and references therein).

Ashin and Nain ophiolitic mélanges are two discrete but similar SSZ-type ophiolites in the northern Nain-Baft ophiolitic belt (Fig. 1b). These ophiolites are also coeval with the Torbat-e-Heydarieh and Sabzevar ophiolites (~ 99, 107 Ma; Fig. 1b) within the Sabzevar-Torbat-e-Heydarieh belt along the northern periphery of the (CIM), whose palaeogeographic evolution within the larger Neo-Tethyan realm was different from that of the Zagros ophiolites along the Zagros thrust zone. The youngest magmatic events in Ashin and Nain ophiolites are recorded by $^{40}Ar/^{39}Ar$ ages of Nain hornblende gabbro (101.2±0.9, 99.7±0.9, 99±1.2 Ma; Hassanipak and Ghazi, 2000), K-Ar age of amphibole in Nain ophiolitic gabbro (93.4±3.6 Ma; Moghadam et al., 2009), K-Ar age for Ashin ophiolite plagiogranite (98 Ma; Sharkovski et al., 1984), as well as biostratigraphic ages for pelagic radiolarian cherts overlying the pillow lavas in Ashin (~ mid-Albian to Turonian (107-94 Ma), Shirdashtzadeh et al., 2015) and Nain ophiolites (~ Albian-Cenomanian (~ 103-93 Ma), Pirnia et al., 2020). These biostratigraphic ages are similar to those reported from other Neo-Tethyan ophiolite localities in Turkey and Iran (e.g., Khoy, Kermanshah, Neyriz, and Soulabest), and southern Tibet (Shirdashtzadeh et al., 2015).

Ashin Ophiolite

The Ashin (or Ashin-Zavar) ophiolitic mélange is a remnant of Ashin-Nain-Baft Neo-Tethyan oceanic crust. Ashin ophiolitic mélange crops out over an area of ~ 100 km^2 along the northwestern margin of the Yazd Block northeast of the Nain Ophiolite, within the Central-East Iranian Microcontinent (Fig. 1b). Similar to most Mediterranean Neo-Tethyan ophiolites of SSZ-harzburgite-dominant type, the Ashin ophiolitic mélange is composed of mantle peridotites (harzburgite, lherzolite, and dunite), serpentinites, chromitites, gabbros, diabase dikes, pillow lavas, and plagiogranites (Shirdashtzadeh et al., 2010; 2011; 2014a; 2014b; Torabi et al., 2011) (Fig. 2, Fig. 1S-a and 1S-e).

The Ashin pillow lavas (Fig. 1S-b) are covered by pelagic *Globotruncana* limestones, radiolarian cherts, and volcanoclastic sediments. In most localities, the pillow lava/dike succession and the overlying sedimentary cover are unmetamorphosed, but pillow lavas are partially altered. Portions of the Ashin (and Nain) ophiolitic sequence experienced metamorphism to produce amphibolites (~ 650-800°C/0.7-0.8Gpa; Shirdashtzadeh et al., 2010), metaperidotites (~ 630-700°C/0.7-1.5Gpa, Shirdashtzadeh et al., 2014b), meta-cherts, and marbles (Fig. 2). This high-grade metamorphism

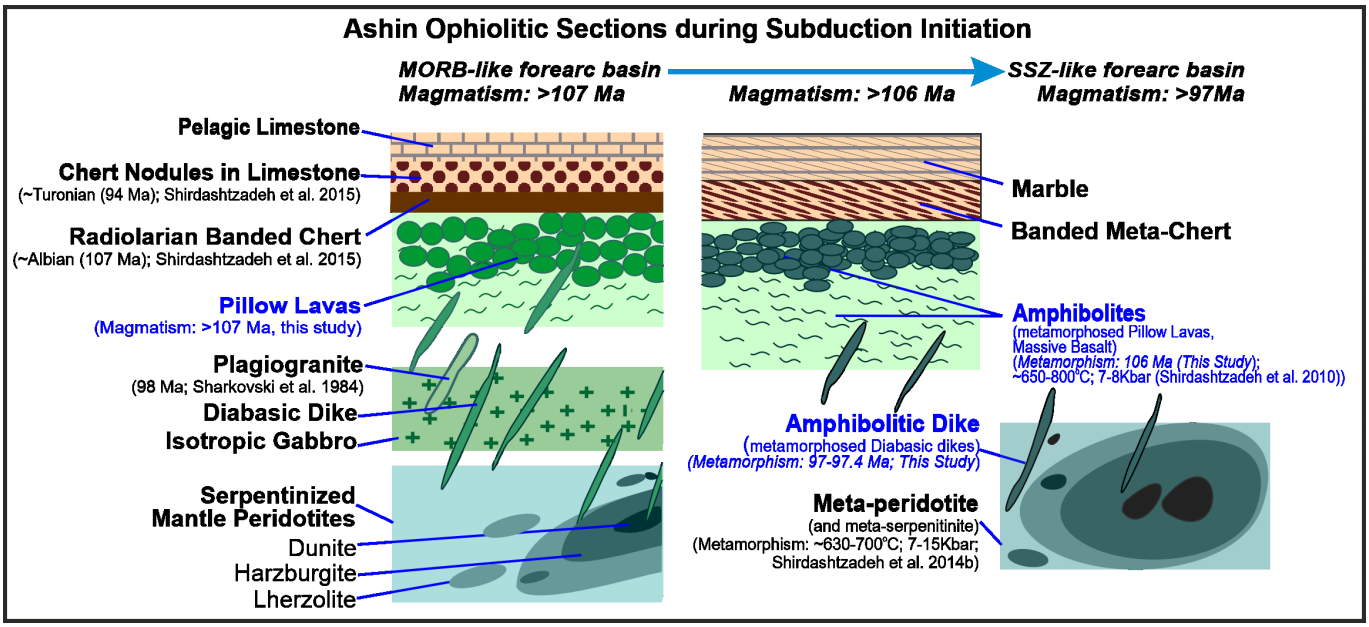

Fig. 2 - Simplified stratigraphic sections of Ashin ophiolite (not to scale).

affected some pillow lavas (now amphibolites), diabase dikes (now amphibolitic dikes), limestones (now marble), and meta-cherts (Fig. 2). In the metamorphosed portions of the mélange, the amphibolites are massive rocks (Fig. 1S-c), whereas amphibolitic dikes are fine-grained, associated within serpentinized mantle peridotites (Fig. 1S-d). Some amphibolitic dikes are partially altered into rodingite.

PETROGRAPHY

We collected amphibolites, amphibolitic dikes, and pillow basalt samples from different localities of the Ashin ophiolitic mélange at Chah-e-Senjed, between Chah-e-Logheh and Douzakh-Dareh (Fig. 1S). Approximate locations of samples are shown in Fig. 1S.

Amphibolites and amphibolitic dikes

found in contact with metamorphosed sedimentary rocks (e.g., meta-cherts and marbles; Fig. 1S-c). The amphibolitic dikes (metamorphosed diabase dikes) are dark green and foliated fine-grained rocks that intruded the serpentinized mantle peridotites (Fig. 1S-d). Both amphibolites and amphibolitic dikes similarly show granoblastic and nematoblastic microscopic textures. Major minerals are pleochroic green hornblende, plagioclase, and clinopyroxene associated with secondary epidote, titanite, chlorite, quartz, and opaque minerals (Fig. 3a-b). These rocks are ortho-amphibolites given the absence of biotite and calcium-rich minerals (e.g., calcite, aragonite, and wollastonite), low modal quartz contents (<< 5 vol%), and presence of magmatic clinopyroxene relicts. Subhedral clinopyroxenes are mostly replaced by amphiboles. However, small colorless to pale-green clinopyroxenes are preserved as relict igneous minerals in some amphibolite samples (Fig. 3b; Fig. 2S). Titanite, calcite, prehnite, and epidote occur as retrograde products of sub-seafloor greenschist metamorphism. Sub- to euhedral plagioclase crystals have undergone retrograde saussuritization into albite, calcite, prehnite, epidote, and chlorite.

Pillow Lavas

Pillow lavas are dark green to brown with characteristic rounded to ellipsoidal pillows 0.5 to 2 meters across (Fig. 1S). These basaltic pillows contain lath-shaped plagioclase, clinopyroxene and olivine phenocrysts, and euhedral brown chromian spinel. Pillow interiors are porphyritic, with variolitic texture in the chilled margins. Intersertal, intergranular to subophitic textures are common toward pillow cores (Fig. 3c-d). Anhedral clinopyroxenes occupy spaces between sub- to euhedral plagioclase laths (Fig. 3c), indicating that plagioclase crystallized first. Clinopyroxenes are partially altered to pumpellyite. Olivines are extremely chloritized (Fig. 3c). Some samples occur as devitrified groundmasses with intersertal textures (Fig. 3d). Chlorite, amphibole, pumpellyite, calcite, and iron oxides occur as secondary minerals, formed by partial devitrification and sub-seafloor greenschist metamorphism.

ANALYTICAL METHODS

From thin section inspection, the rodingitized and altered samples were ignored and representative samples selected for geochemical analyses. Details of the analytical procedures and instruments are presented in Supplementary text S1. Based on petrographic observations in a representative amphibolite, clinopyroxene remnants were selected for LA-ICP-MS analysis (Table 1S). LA-ICP-MS data for clinopyroxenes in pillow lavas are from Shirdashtzadeh et al. (2014a) (Table 2S). To determine the tectonomagmatic setting of rocks, in addition to the published dataset (Table 2S), three amphibolitic rocks and two representative pillow lava samples were selected for whole-rock geochemistry (Table 3S). Furthermore, to investigate the melt source isotopic nature, four amphibolite and two pillow lava representative samples were analyzed for Sm-Nd isotope ratios (Table 1). Present-day $^{147}Sm/^{144}Nd = 0.1967$ and $^{143}Nd/^{144}Nd = 0.512638$ ratios for CHUR (Chondritic Uniform Reservoir; DePaolo and

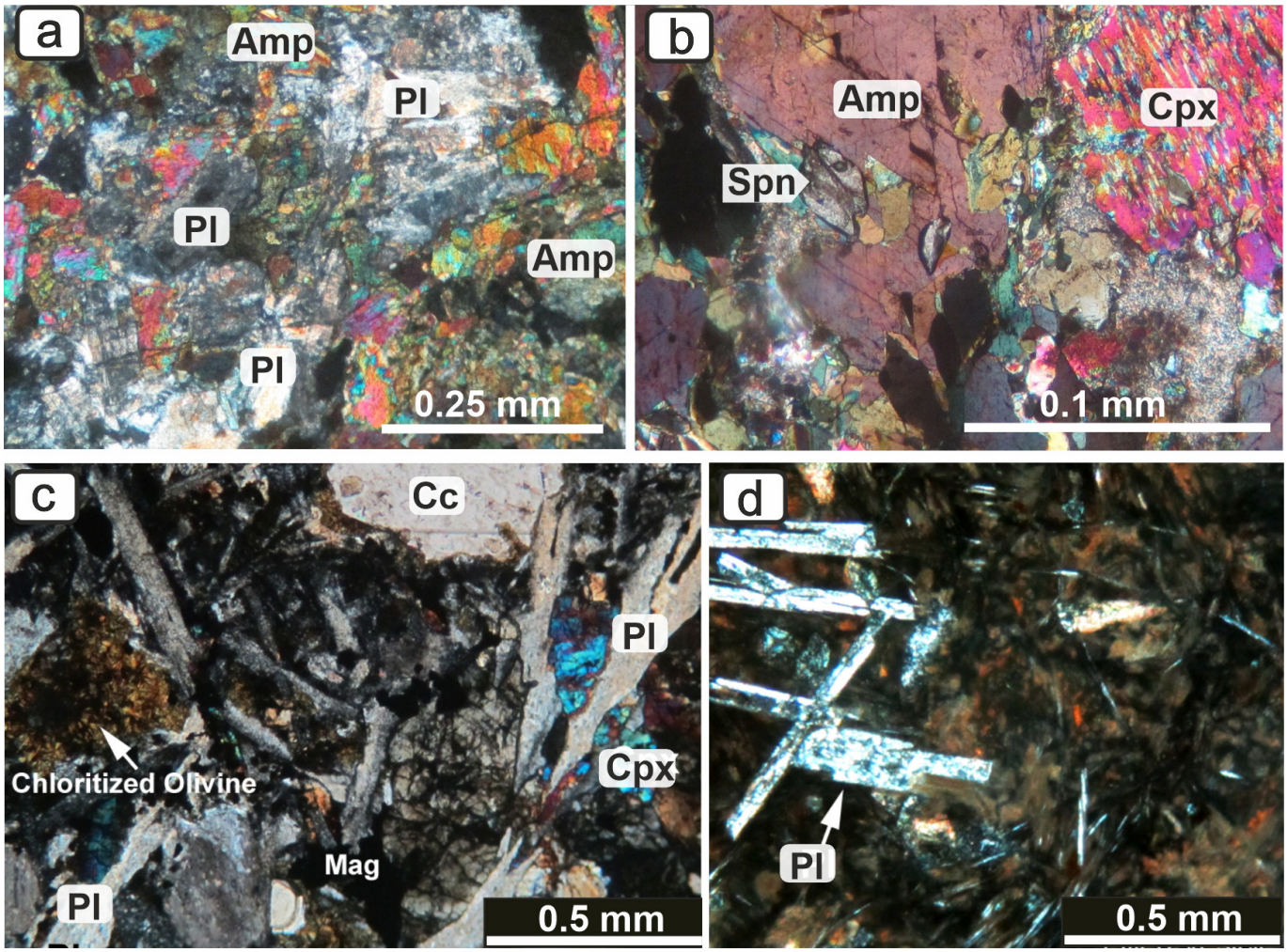

Fig. 3 - Photomicrographs (under cross-polarized light) of (a) amphibole and altered plagioclase in amphibolite; (b) clinopyroxene relics in amphibolite; (c, d) clinopyroxene, altered plagioclase, chloritized olivine in pillow lava with intergranular and intersertal texture. Amp = Amphibole, Cpx = Clinopyroxene, Mag = Magnetite, Pl = plagioclase, Spn = Sphene.

Table 1 - $^{147}Sm/^{144}Nd$, $^{143}Nd/^{144}Nd$ ratios and εNd for amphibolites and basic lavas in Ashin ophiolite.

Sample No.	Lithology	Sm (ppm)	Nd (ppm)	Sm/Nd	$^{147}Sm/^{144}Nd$	$^{143}Nd/^{144}Nd$ (±2σ)	εNd_o	εNd_I	Age (Ma)
A127	Amphibolite	1.807	5.38	0.336	0.2213	0.512932 ±16	5.7	5.7	104
A124	Amphibolite	2.883	7.531	0.383	0.2314	0.513190 ±5	10.8	10.3	104
A102	Amphibolite Dike	3.982	13.81	0.288	0.1744	0.512990 ±3	6.9	7.1	97
A143	Amphibolite Dike	4.221	4.667	0.904	0.5467	0.513131 ±9	9.6	5.3	97
A108	Basic Pillow Lavas	2.4	7.048	0.341	0.2058	0.512839 ±9	3.9	3.8	107
A113	Basic Pillow Lavas	2.997	8.394	0.357	0.2158	0.513058 ±5	8.2	7.9	107

Wasserberg, 1979) were used to calculate εNd_o. Additionally, two representative amphibolitic dikes and one amphibolite sample with minimum alterations in the polished thin section were selected for zircon U-Pb analysis (Table 2). Textural features of zircons in cathodoluminescence (CL) images (Fig. 4S) are used to illuminate zircon origin.

DATA AND RESULTS

Clinopyroxene trace element compositions

In N-MORB (normal mid-ocean ridge basalt)-normalized diagram (Fig. 5), the trace element patterns of clinopyroxenes of Ashin pillow lavas and amphibolites exhibit

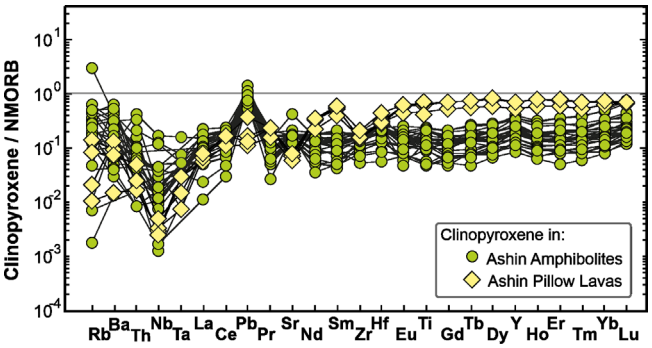

Fig. 4 - Incompatible trace element composition of clinopyroxene from the Ashin amphibolite and pillow lavas normalized to N-MORB. Normalization values from Sun and McDonough (1989).

similar trends. However, clinopyroxene in pillow lavas is characterized by higher high field strength elements (HFSE: Ti, Y, Zr, Nb, Ta) and heavy rare earth elements (HREE), and lower Sr, Pb, Eu/Eu* (mean = 0.96), Ce_N/Yb_N: ~ 0.12-0.15, and Sm_N/Yb_N: ~ 0.42-0.87, compared to amphibolites (Eu/Eu*: mean = 1.2; Ce_N/Yb_N: ~ 0.13-1.24, Sm_N/Yb_N: ~ 0.14-1.25; Table 1S and 2S). Based on the absolute Nb and Th concentrations, some clinopyroxenes in amphibolite seem to be as depleted as those in the pillow lavas, however, amphibolite clinopyroxenes display a broader spectrum in Nb and Th, covering the ranges defined by the pillow lavas. In addition, most amphibolite samples remain enriched relative to the pillows. Lower Yb and Zr in the amphibolites create a larger variation of Nb/Yb and Nb/Zr ratios than pillow lavas.

Whole rock elemental and Nd isotopic compositions

Whole rock major, minor, and trace element contents and Nd isotopic compositions for amphibolitic rocks and pillow lava samples of the Ashin ophiolite are presented in Table 3S and Table 1. Amphibolitic samples often show compositional overlap with pillow lavas in major, rare earth and trace elements and Nd isotopes. Ashin pillow lavas have SiO_2 contents ranging from 45 to 54 wt% (Total alkali: 3.6-5.9 wt%; TiO_2: 1-1.5 wt%; MgO: 2.6-9.4 wt%; CaO: 5.8-14.5 wt%; $^{143}Nd/^{144}Nd$ of ~ 0.512839-0.513058; εNd_I = +3.8 to +7.9). Ashin amphibolites and amphibolitic dikes are characterized by SiO_2 ranging from 47 to 55 wt% (Total alkali: 2-5.6 wt%; TiO_2: 0.5-1.8 wt%; MgO: 3.4-8.8 wt%; CaO: 7.5-16.6 wt%; $^{143}Nd/^{144}Nd$ of ~ 0.512932-0.513190; εNd_I of +5.3 to +10.3). In N-MORB-normalized trace element diagrams, pillow lavas (Fig. 5a), amphibolites (Fig. 5b), and amphibolitic dikes (Fig. 5c), exhibit flat REE (except La and Ce that show broader spectrums, notably in the amphibolitic dikes), enrichment in Pb, Th, and large ion lithophile element (LILE: Rb, Ba, Sr), and negative HFSE anomalies (Nb, Ta, and Zr). Amphibolitic dikes, however, show lower REE and higher K, Sr, and Rb concentrations (Fig. 5).

The protoliths of the amphibolite and amphibolitic dike samples were mainly mafic mantle-derived magma based on high Na_2O/Al_2O_3 and low Zr/Ti (Fig. 6a-b), the high εNd_I value (mean: +7.1, n = 4) and low Th/Ce ratio (mean: ~ 0.03, n = 5) (Table 1; Table 3S). The major and trace element compositions are consistent with a sub-alkaline basalt to andesite protolith (Fig. 6c-d).

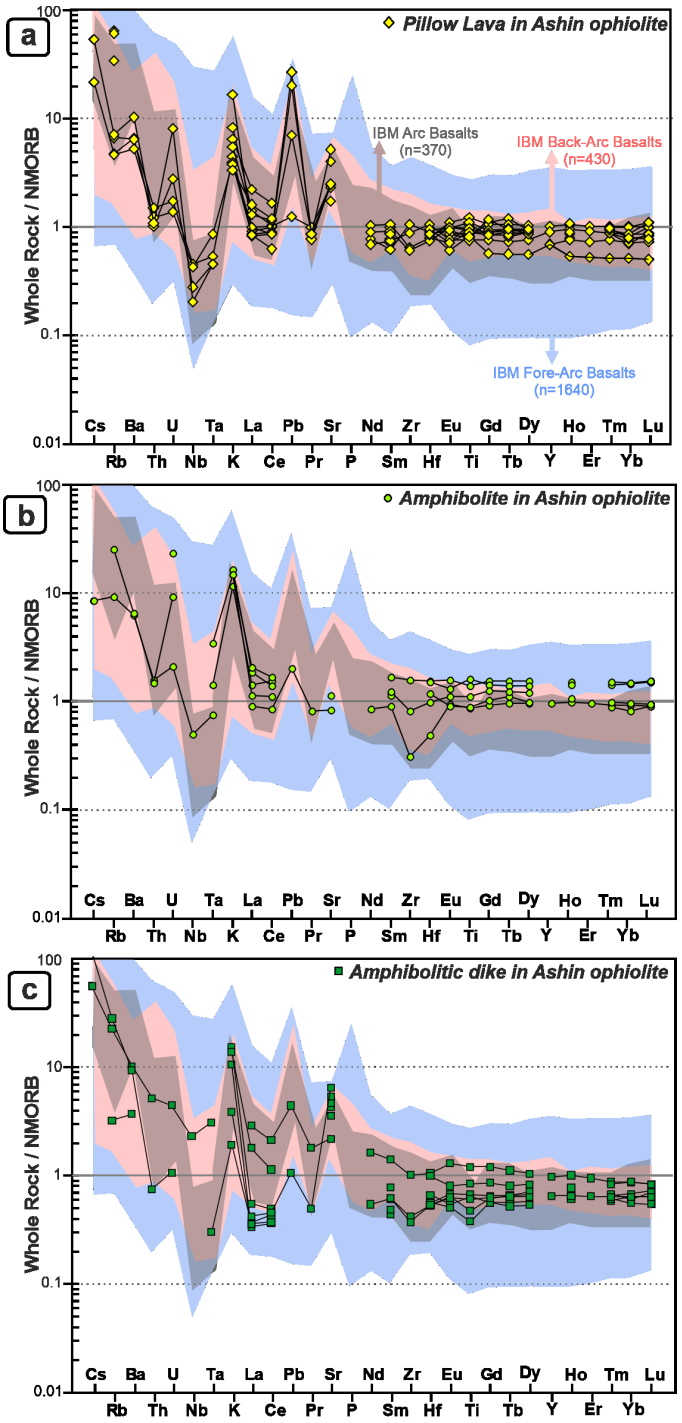

Fig. 5 - N-MORB-normalized patterns of (a) pillow lavas, (b) amphibolites, and (c) amphibolitic dikes from the Ashin ophiolite. Normalization values of N-MORB from Sun and McDonough (1989). Database and references for IBM fore-arc, arc and back-arc basalts from GEOROC database (http://georoc.mpch-mainz.gwdg.de).

Zircon composition, morphology, and U-Pb ages

High Th/U ratios zircons from Ashin ophiolite amphibolitic dikes (0.44-0.91) and Ashin amphibolites (0.12-0.27) are consistent with both magmatic zircons and UHP-UHT metamorphic zircons (see Fig. 3S). Lower Th/U ratios of zircons in some Ashin amphibolites (0.04-0.07) are consistent with the LT-PT metamorphic zircons (Fig. 3S).

Table 2 - U and Pb isotopic data for the zircons in the amphibolitic rocks.

Sample No.	Th/U	$^{206}Pb/^{204}Pb$	1σ%	$^{207}Pb/^{206}Pb$	1σ%	$^{207}Pb/^{235}U$	1σ%	$^{206}Pb/^{238}U$	1σ%	Rho	$^{207}Pb/^{206}Pb$	2σ abs	$^{206}Pb/^{238}U$	2σ abs	$^{207}Pb/^{235}U$	2σ abs
Amphibolite:																
A135-ZR01	0.14	3870	10.79	0.04911	5.67	0.113	5.95	0.0167	1.76	0.3	153	255	107	4	109	12
A135-ZR02	0.04	4130	6.79	0.05098	3.11	0.102	3.53	0.0149	2.58	0.73	240	140	100	2	106	7
A135-ZR03	0.04	3009	13.85	0.05081	5.47	0.119	5.98	0.0169	2.39	0.4	232	243	108	5	114	13
A135-ZR08	0.26	5889	9.69	0.05171	2.53	0.115	2.71	0.0162	0.91	0.34	272	114	103	2	111	6
A135-ZR11	0.04	4703	10.37	0.05042	2.67	0.11	3.24	0.0158	1.8	0.55	214	121	101	4	106	6
A135-ZR12	0.22	11275	29.25	0.05488	1.47	0.124	1.73	0.0165	0.84	0.48	407	65	105	2	119	4
A135-ZR13	0.12	5935	14.61	0.04969	3.66	0.108	4.16	0.0158	1.95	0.47	181	166	101	4	104	8
A135-ZR14	0.07	5576	10.07	0.05092	2.45	0.115	2.63	0.0164	0.89	0.34	237	111	105	2	111	6
A135-ZR15	0.22	3877	7.73	0.04818	2.37	0.108	2.62	0.0163	1.05	0.4	108	110	104	2	105	5
A135-ZR16	0.04	4762	17.16	0.05005	2.99	0.116	3.18	0.0168	1.01	0.32	197	136	107	2	111	7
A135-ZR21	0.27	8896	16.14	0.05408	1.64	0.123	1.81	0.0164	0.67	0.37	374	73	105	1	117	4
Amphibolitic Dike:																
A142-ZR01	0.6	66029	24.71	0.04834	0.59	0.1	0.93	0.015	0.61	0.66	116	28	96	1	97	2
A142-ZR02	0.9	39004	26.45	0.04823	0.97	0.101	1.22	0.0152	0.63	0.52	111	46	97	1	98	2
A142-ZR05	0.91	57549	33.35	0.04946	0.94	0.105	1.15	0.0154	0.54	0.47	170	44	99	1	101	2
A142-ZR06	0.54	46610	20.54	0.04808	0.94	0.101	1.24	0.0153	0.71	0.58	103	44	98	1	98	2
A144-ZR03	0.69	18251	22.83	0.04878	0.89	0.104	1.49	0.0154	1.14	0.76	137	42	99	2	100	3
A144-ZR05	0.58	22742	21.08	0.04861	1.03	0.103	1.31	0.0154	0.72	0.55	129	48	98	1	100	2
A144-ZR06	0.61	33495	17.31	0.04872	0.71	0.106	1.68	0.0158	1.48	0.88	134	33	101	3	103	3
A144-ZR07	0.44	35986	27.68	0.04838	0.71	0.101	1.74	0.0152	1.55	0.89	118	33	97	3	98	3
A144-ZR08	0.64	55012	24.59	0.04668	0.77	0.097	1.1	0.015	0.68	0.62	33	37	96	1	94	2
A144-ZR10	0.44	14685	22.91	0.04869	1.2	0.101	1.53	0.015	0.87	0.57	133	56	96	2	98	3

Calculations were done using CHRONUS (Version 1.4.3) by Felipe Valença. Decay constants of Jaffey et al. (1971). References are reported in Supplementary text S2

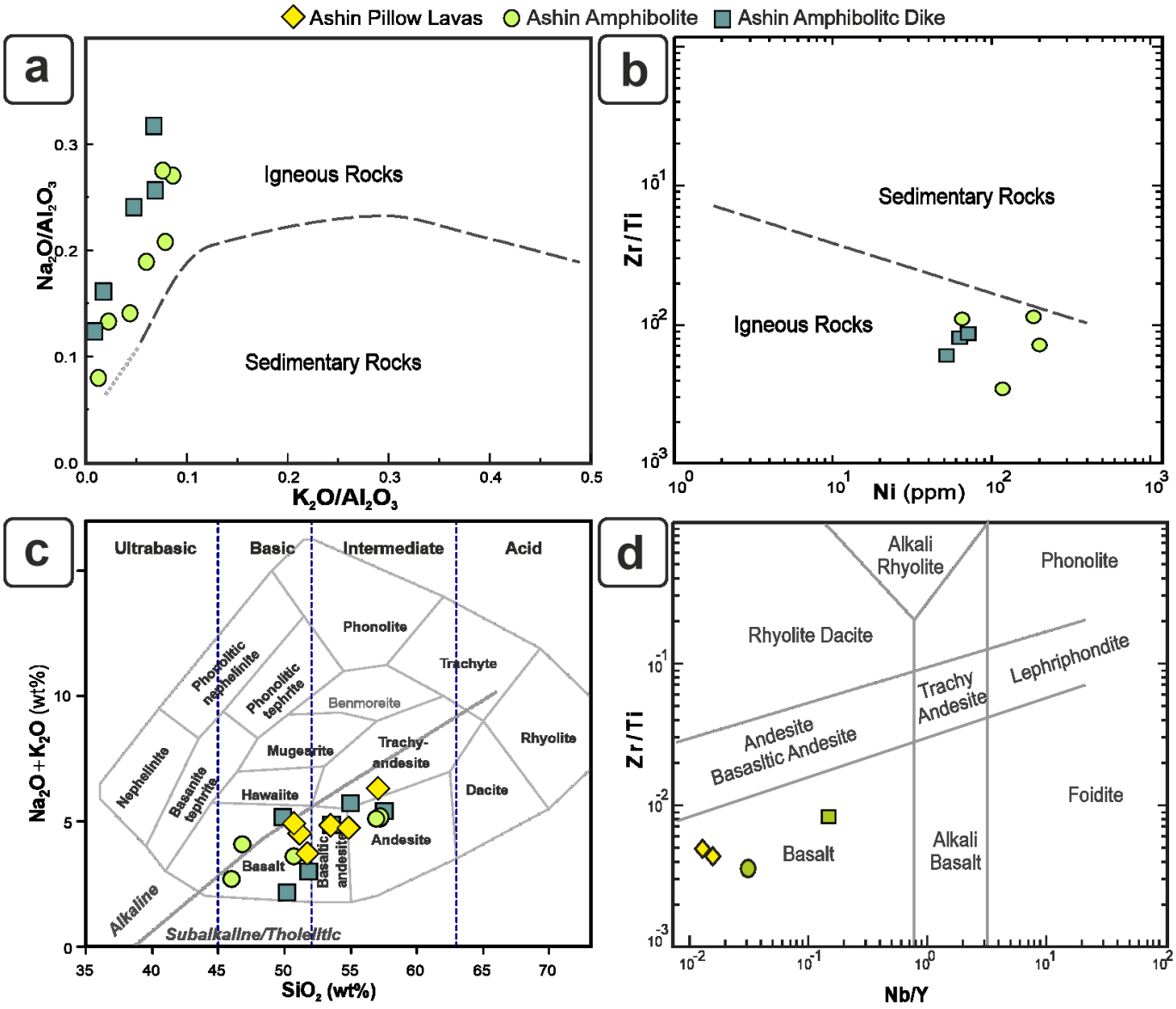

Fig. 6 - (a) Binary plot of K_2O/Al_2O_3 versus Na_2O/Al_2O_3 (discrimination line after Garrels and Mackenzie, 1971); (b) Ni versus Zr/Ti diagram (discrimination line after Winchester et al., 1987); (c) SiO_2 versus Na_2O+K_2O (fields and nomenclature after Cox et al., 1979); (d) Nb/Y versus Zr/Ti diagram (fields and nomenclature after Winchester and Floyd, 1977).

Textural features of zircons in cathodoluminescence (CL) images are often used in addition to Th/U ratios to constrain the origin of zircon (e.g., Corfu et al., 2003; Hu et al., 2017; Rubatto, 2017). Zircons of the amphibolitic dike have subhedral to anhedral shapes (Fig. 4S) and exhibit weak and patchy CL zoning without indications of inherited cores. Amphibolite zircons often have anhedral shapes and lack CL zoning, consistent with 'metamorphic zircons' recrystallized and homogenized at granulite facies (e.g., Corfu et al., 2003) and estimated P/T conditions that could reset the U-Pb system of zircons in amphibolitic rocks (~ 650-800°C/0.7-0.8 GPa; Shirdashtzadeh et al., 2010). Metamorphic zircons in the amphibolites have a mean U-Pb age of ~ 104 Ma (Fig. 7a), indicating that their igneous protolith is older than ~ 104 Ma. The mean U-Pb ages of magmatic zircons in the amphibolitic dikes is consistent with younger ages (~ 97.3 Ma, Fig. 7b; 97.4 Ma, Fig. 7c) for their igneous protolith.

DISCUSSION

Below, we use our new data to discuss two issues: 1) Tectonomagmatic origin of Ashin pillow lavas and amphibolites; and 2) A revised model for the Mesozoic Ashin ophiolites: subduction initiation.

Tectonomagmatic origin of Ashin pillow lavas and amphibolites

Whole rock geochemical signature of subduction initiation setting

Rocks from SSZ ophiolites have differing geochemical characteristics (Furnes et al., 2014) due to the maturity of the subduction systems in which they developed. This is caused by various extent of subduction zone enrichment by fluid or melt contributions from the sinking slab and overlying sediments during subduction initiation, resulting in extrusive rocks ranging from MORB to IAT (island arc tholeiite),

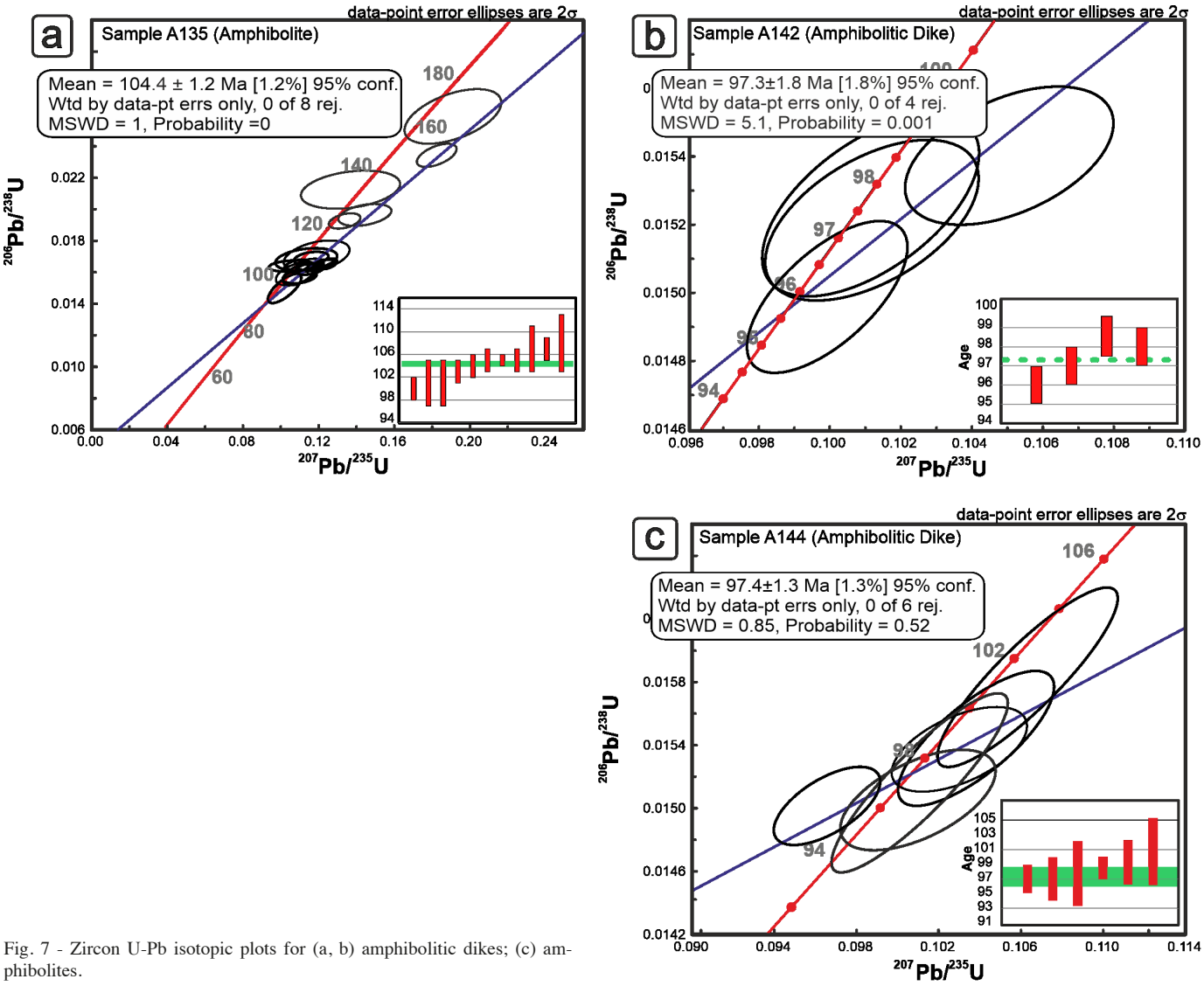

Fig. 7 - Zircon U-Pb isotopic plots for (a, b) amphibolitic dikes; (c) amphibolites.

and boninite (Dilek and Furnes, 2009; Dilek and Thy, 2009; Whattam and Stern, 2011).

Some trace elements as well as rare earth elements and Nd isotopes are useful tracers of petrogenetic processes. At the time FAB formed, there was no existing arc and subsequently back arc basin, because a subduction-related island arc does not start to form until several million years after subduction initiation (Shervais et al., 2019). Therefore, distinguishing the tectonomagmatic setting of magma is a clue to explain the timing of a subduction zone. To assess the tectonomagmatic setting within the Neo-Tethys oceanic realm, we compare Ashin pillow lavas (non-metamorphosed basic rocks) and amphibolites (metamorphosed basic rocks) to the compiled trace elements and Nd isotopes dataset of IBM FAB, arc, and BAB settings.

In N-MORB (normal mid-ocean ridge basalt)-normalized diagrams, REE (excluding La and Ce), Zr, Ti, and Hf contents are 0.5 to 1 times depleted in Ashin amphibolitic dikes and pillow lavas, while they are 1 to 2 times enriched in the amphibolites (Fig. 5c). Nevertheless, REE (excluding La and Ce), Zr, Ti, and Hf contents are similar to those of normal MORB lavas formed in mid-oceanic ridges, whereas the positive spikes for Cs, Rb, Ba, U, K, and Sr together with negative Nb and Ta anomalies (Fig. 5) are similar to those in subduction-related lavas (FAB, arc, and BAB) lavas (e.g., Kelemen et al., 2007; Zheng, 2019; Xia and Li, 2019). FAB rocks span a wider HFSE and LILE range than arc and BAB; however, the normalized spider patterns are not diagnostic for various SSZ tectonic settings because the Ashin samples, IBM FAB, arc, and BAB show trace and rare earth element compositional overlap (Fig. 5).

The Ashin amphibolitic rocks and pillow lavas as well as IBM FAB dataset mostly contain lower Sm, Zr and MgO than MORB and lower MgO than boninite (Fig. 8a-b). Ti versus V plot (Fig. 8c) is another common diagnostic plot used for constraining tectonic settings of modern and ophiolitic volcanic rock as well as distinguishing MORB, island arc tholeiite (IAT) and boninite magma types (e.g., Shervais, 1982; Pearce, 2014). As a function of the fO_2 of the magma, partial melting, and fractional crystallization, Ti/V ratios are ~ 20 for arc volcanics, 20-50 for MORB and continental flood basalts, and 10 to 50 for arc-like or MORB-like BAB (Shervais, 1982), whereas it is ~ < 10 to 50 for arc to oceanic floor basalts for IBM FAB (Fig. 8c-d). Within the IBM FAB field, Ashin amphibolitic dikes (Ti/V ~ 10-20) lie in the more oxidized arc field (Fig. 8c) whereas amphibolites and pillow

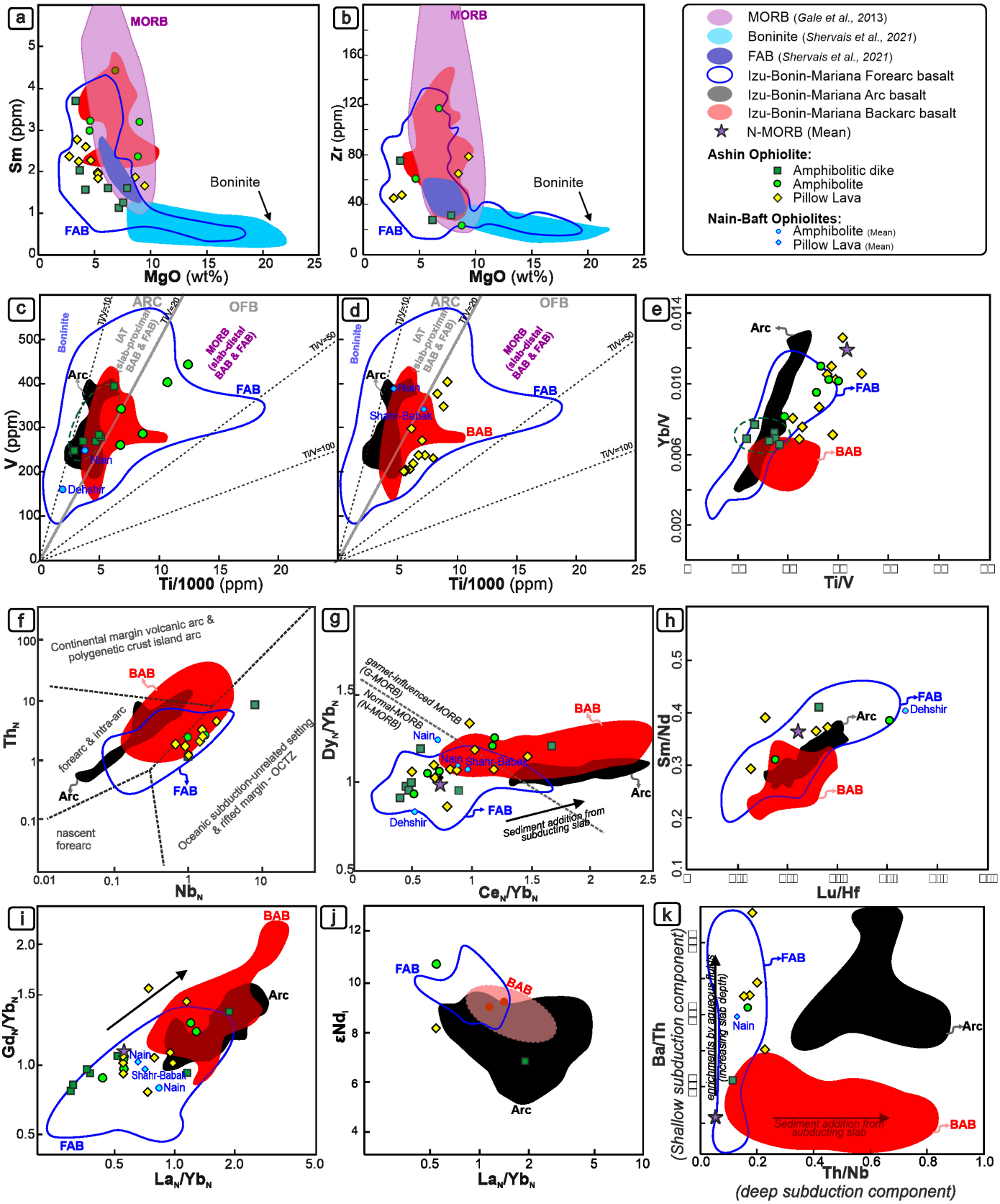

Fig. 8 - Ashin amphibolites, amphibolitic dikes, and pillow lavas: (a, b) MgO versus Sm and Zr (modified after Shervais et al., 2021); (c, d) Ti versus V (Shervais, 1982; Pearce, 2014); (e) Ti/V versus Yb/V; (f) Nb_N versus Th_N (Saccani, 2015); (g) Ce_N/Yb_N versus Dy_N/Yb_N (Saccani, 2015); (h) Lu/Hf versus Sm/Nd; (i) La_N/Yb_N versus Gd_N/Yb_N; (j) La_N/Yb_N versus εNd_I; (k) Th/Nb versus Ba/Th; N: Normalization values for N-MORB after Sun and McDonough (1989). Data for IBM fore-arc (FAB), arc and back-arc (BAB) basalts from GEOROC database (http://georoc.mpch-mainz.gwdg.de).

lavas (Ti/V ~ 20-50) lie in the field of less oxidized magmas (Fig. 8c-d). Reagan et al. (2010) suggest that Ti/V and Yb/V ratios are generally lower in FAB than BAB and MORB. However, in the Ti/V versus Yb/V plot, Ashin samples are in the FAB field, showing a slightly elevated Yb/V ratio to BAB and elevated Ti/V to arc (Fig. 8e).

In the N-MORB normalized Th_N versus Nb_N diagram of Saccani (2015), BAB rocks with lower Nb and Th contents overlap with FAB and some arc rocks (Fig. 8f). Ashin samples plot outside of the arc field but within the FAB and BAB composite fields. Ce_N/Yb_N versus Dy_N/Yb_N plot may reflect mantle LREE/HREE enrichment in BAB and arc rocks due to addition of sediment melts and fluids from the subducting slab (Fig. 8g). Ashin samples are mainly distributed in the FAB field with the lowest LREE/HREE (Ce_N/Yb_N <~ 1.5), indicating the lowest addition of sediment melts and fluids from the subducting slab. The FAB-like mantle source of Ashin samples is similar to normal depleted MORB-type mantle (DMM) at shallow levels rather than a G-MORB (i.e., "garnet-influenced MORB" in Saccani 2015) (Fig. 8g), analogous to a subduction initiation with little enrichment by slab-derived materials. Reagan et al. (2010) speculate that mantle upwelling associated with subduction initiation caused cpx-rich domains with high Sm/Nd and Lu/Hf to melt to generate FAB. Thus, Lu/Hf and Sm/Nd ratios may be slightly higher for FAB melts during subduction initiation than metasomatized BAB melts above a mature subduction zone (Fig. 8h).

Ashin amphibolitic rocks and pillow lavas as well as FAB and N-MORB rocks have lower Gd_N/Yb_N and La_N/Yb_N (Fig. 8i) than arc and BAB basalts. Slab-derived materials increased LREE/HREE of BAB and arc mantle sources, while low LREE/HREE of FAB indicate depleted mantle contribution with lesser subduction-input.

The whole rock εNd_I of IBM BAB is in the range of IBM FAB and arc rocks, however, FAB (εNd_I >~ 8) and then BAB (εNd_I >~ +7.5) rocks are higher than arc in initial εNd (Fig. 8j). The Ashin pillow lava (εNd_I: +3.8, +7.9) and amphibolite (εNd_I: +5.7, +10.3) plot close the range of IBM FAB to BAB rocks, but the amphibolitic dike (εNd: +5.3, +7.1) is within the arc field (Fig. 8j).

Ratios of elements of similar incompatibilities, one subduction-mobile, and one subduction-immobile, highlight subduction inputs (Pearce et al., 2005). The Th/Nb, Ba/Th (and Th/Nb and Ba/Nb; not shown) ratios provide useful petrogenetic insights to the subduction zones (Fig. 8k). Ashin amphibolites and pillow lavas show high Ba/Nb and Ba/Th ratios (Fig. 8k) similar to FAB rocks reflecting shallower and cooler fluid components (Pearce et al., 2005). Ashin samples are compositionally distinct from BAB basalts that are characterized by high Th/Nb ratio due to sediment melt addition from deep subducting lithosphere (Fig. 8k). They are also distinct from arc rocks that contain high Th/Nb and Ba/Th ratios (Fig. 8k) known as total subduction components (Pearce et al., 2005).

Whole rock chemistry (e.g., low LREE/HREE and Th/Nb, high Ti/V, Ti/Yb, and Ba/Th, Fig. 8) indicates that the Ashin pillow lavas (~ 107 Ma) and igneous protolith of amphibolites (~ 104 Ma) were neither backarc basalts nor calc-alkaline volcanic rocks. They most likely formed in an early subduction initiation MORB-like FAB zone, while the igneous protolith of amphibolitic dikes occurred in a younger (~ 97 Ma) and subsequently more developed FAB subduction setting with higher slab fluid contributions and subsequent SSZ geochemical affinities (e.g., lower Ti/V and Ba/Th, Fig. 8c, d, k).

Clinopyroxene signature of subduction initiation setting

Trace element compositions of clinopyroxene relicts provide another key to constrain the tectonic setting of the Ashin mafic samples. Clinopyroxenes in Ashin amphibolites and pillow lavas have contrasting REE and trace element compositions, suggesting different tectonomagmatic settings (Fig. 4). Clinopyroxenes in Ashin amphibolites exhibit a wider range of Ce_N/Yb_N (0.13-1.24) and Sm_N/Yb_N (0.14-1.25) than pillow lavas (Ce_N/Yb_N: 0.12-0.15; Sm_N/Yb_N: 0.42-0.87).

Asthenospheric mantle in the proto-subduction zone region (i.e., FAB) is not oxidized before subduction initiation. Therefore, depleted mantle in an early subduction initiation zone is not as oxidized as more SSZ-like FAB mantle that evolves later during subduction initiation or younger subduction-modified mantle wedge above the subducting slab in a BAB setting. Regarding the crystallization priority of feldspars (that capture abundant Eu^{2+}) rather than clinopyroxene in a MOR setting and their vice versa crystallization priority in a SSZ setting, the Eu anomaly increases from Ashin pillow lavas (mean: 0.96 (n = 4); Table 2S) to amphibolites (mean Eu/Eu*: 1.2 (n = 30); Table 1S), indicating that the magma setting is changing from a MOR-like FAB to a SSZ-like FAB. In fact, in subduction-related magmas, clinopyroxene crystallizes before plagioclase, whereas the opposite occurs for N-MORB (e.g., Hebert and Laurent, 1990), similar to a MORB-like FAB developed early during subduction initiation. If plagioclase crystallized before clinopyroxene (Fig. 3c-d) in a Eu^{2+}-rich MORB-like FAB system, clinopyroxene would capture less Eu^{2+} than plagioclase, as it seems to be the case for Ashin pillow lava clinopyroxenes that show negative Eu anomalies. In the case of Ashin, the Eu^{3+}/Eu^{2+} ratio of clinopyroxenes should progressively increase from pillow lavas to amphibolites because of progressive oxidation of the mantle associated with subduction initiation progress until the establishment of a mature subduction zone (Whattam and Stern, 2011).

Cretaceous subduction initiation of eastern Neo-Tethys oceanic crust

The eastern Neo-Tethyan ophiolite relicts along Nain-Baft ophiolitic Belt exposed by the Zagros Orogen (Fig. 1) were affected by a wide variety of magmatic and metamorphic events during multiple stages of Mesozoic rifting and subduction (e.g., Sharkovski et al., 1984; Mattei et al., 2014; Pirnia et al., 2020; Shirdashtzadeh et al., 2010; 2011, 2014b; 2015; 2020). Each event gives a clue to reconstructing the tectonic setting of birth to death of Neo-Tethys oceanic crust in Central Iran. Previous studies considered some lavas in the eastern Neo-Tethys oceanic basin to be formed in SSZ FAB, arc, to BAB settings (e.g., Table 1 in Moghadam and Stern, 2015). The average composition of Cretaceous Nain and Shahr-Babak lavas together with Nain and Dehshir amphibolites from Nain-Baft ophiolitic belt (Fig. 8c, d, g, i, and k) yields MORB-like to SSZ-like "forearc" affinity rather. It suggests that the eastern Neo-Tethys subduction initiation along Nain-Baft ophiolitic belt occurred in the late Early Cretaceous (~ 107-97Ma).

The time required to establish a back-arc spreading basin is estimated to be ~ 55 Myrs (Molnar and Atwater, 1978; Sdrolias and Müller, 2006; Goes et al., 2017); however, formation of some younger back-arc basins are ascribed to ~ 23-15 Myrs (Van Horne et al., (2017) and references therein) and < 15 Myrs (e.g., ~ 4-6 Ma (Andaman Backarc Basin; Yatheesh et al., 2021); ~ 3.5-4 Myrs (Lau Basin; Malahoff et al., 1982; Martinez and Taylor, 2002); ~ 10 Ma (Sea of

Japan and Lau-Havre-Taupo Basin; Van Horne et al. (2017) and references therein). The biostratigraphic ages of radiolarian cherts (Shirdashtzadeh et al., 2015), as well as our geochronological data, indicate that the forearc basin in the Ashin area formed in the mid-Cretaceous (~ 107 to 97 Ma). If we postulate an Early to Middle Jurassic age for the subduction initiation (Cimmerian Orogeny, ~ 185-180 Ma; e.g., Fergusson et al., 2016) of the western Neo-Tethys oceanic crust, then the eastern Neo-Tethys oceanic spreading might be initiated as its backarc basin in ~ 55 Myrs later in Early Cretaceous (~ 130-125 Ma). Unsurprisingly, the Nain-Baft ophiolites have occurred earlier at Jurassic time (e.g., gabbro in Kahnuj: 156 Ma, Kananian et al., 2001). Thus, the eastern Neo-Tethys ocean could not be formed as a backarc basin of eastward subducting slab of western Neo-Tethys oceanic crust, because the subduction-related arc of the western oceanic basin was not formed yet.

Oligocene-Miocene Andean-type subalkaline magmatism in Urumieh-Dokhtar magmatic arc is ascribed to Cretaceous eastward subduction of Neo-Tethys oceanic crust beneath Sanandaj-Sirjan Zone and Central-East Iranian Microcontinent during continuous Cenozoic-Quaternary convergence of the Arabian and Iranian plates (e.g., Berberian and Berberian, 1981; Azizi and Moinevaziri, 2009; Yeganehfar et al., 2013; Zheira et al., 2020). However, if the western oceanic basin was a backarc then it should be younger than the arc system of Urumieh-Dokhtar magmatic arc, but this is not the case. The NW-SE trend of Oligocene-Miocene subduction-related continental magmatic arc of Urumieh-Dokhtar magmatic arc that is crossing the Nain-Baft ophiolitic belt in the south of Nain and north of Dehshir ophiolites (Fig. 1b) indicate that Nain-Baft Neo-Tethayn oceanic crust certainly closed a few tens of million years (before the Eocene-Oligocene, likely in ~ Late Cretaceous-Paleocene) before the closure of the western oceanic basin of the Neo-Tethys oceanic crust (in the l

Sub-sea floor metamorphism in the Cretaceous oceanic crust

The pillow lavas are usually supposed to occupy the upper portion of the oceanic lithosphere. In Ashin ophiolite, the petrographic observations and mineralogy of pillow lavas (devitrification and secondary minerals of chlorite, amphibole, pumpellyite, calcite, and iron oxides; Fig. 3c-d) support the metamorphic grade as greenschist facies. Ashin pillow lavas have experienced a low-temperature metamorphic condition at greenschist facies, because they were generated in an early forearc basin with a relatively cool thermodynamic condition (about 450°C; Hyndman, 2019) and a maximum geothermal gradient of no more than 30°C/km (Allen and Allen, 1990).

While Ashin pillow lavas have formed in a cool forearc basin in Cretaceous (104 to 97 Ma), the Ashin amphibolites and amphibolitic dikes were affected by a medium- to high-grade sub-seafloor metamorphism at amphibolite-granulite facies (~ 650-800°C/0.7-0.8 GPa to ~ 630-700°C/0.7-1.5 Gpa; Shirdashtzadeh et al., 2010: 2014b), recorded in zircons by low Th/U ratio (Fig. 3S) and the petrographic observations (e.g., clinopyroxenes replaced by amphiboles; Fig. 3a-b). This high-temperature metamorphism may occur in an oceanic thrust-faulted zone, island arcs, fracture zones, or a mature subduction zone with a thermally weakened lithosphere (e.g., subduction backarc), rather than later heating during continental collision orogeny (Hekinian, 1982; Hyndman, 2019).

A revised model for mid-Cretaceous Ashin (and Nain) ophiolites: subduction initiation

Jurassic oceanic rocks, including radiolarians (Kojima et al., 1994), pillow and massive lavas (Bortolotti et al., 2018; Jahangiri et al., 2020), diabasic dikes (Zhong et al., 2006; Balci and Sayit, 2020), trondhjemites (Topuz et al., 2013; Moghadam and Stern, 2015), gabbros (Pedersen et al., 2001; Kananian et al., 2001; Rolland et al., 2010; Alparslan and Dilek, 2018), and plagiogranites (Dilek and Thy, 2009; Moghadam and Stern, 2015; Shirdashtzadeh, Unpublished Data) are reported from many AHOB ophiolites (Fig. 1a). In addition, the paleomagnetic research (Mattei et al., 2014, and references therein) suggests that Late Triassic-Jurassic spreading followed by Middle Jurassic-Early Cretaceous rotation around the Central-East Iranian Microcontinent. The Jurassic Kahnuj gabbro-diorites (156-146 Ma; Kananian et al., 2001; Fig. 1b) and probabely, the Ashin plagiogranites (188 Ma; Sharkovski et al., 1984) reflect an early oceanic magmatism in a Jurassic Neo-Tethys spreading system. Accordingly, Shirdashtzadeh et al. (2010; 2011) and Torabi et al. (2011) proposed a Jurassic backarc origin for the protoliths of Ashin and Nain amphibolites, and a Cretaceous forearc setting for their non-metamorphosed rocks (i.e. pillow lavas and basic dikes). No support for a Jurassic age for Ashin plagiogranites, however, Shirdashtzadeh et al. (unpublished data) obtained U-Pb Jurassic ages of zircons in plagiogranites from Nain ophiolite. Our new U-Pb and geochemical dataset provides evidence for a Cretaceous oceanic basin for the formation of both metamorphosed (amphibolites and amphibolitic dikes) and non-metamorphosed (pillow lavas) magmatic rocks.

Based on the composition of Nain ophiolite lherzolites (Pirnia et al., 2018), Jurassic ages for the Kahnouj gabbros (Kananian et al., 2001) and Ashin-Nain plagiogranites (Sharkovski et al., 1984), and the paleomagnetic direction results by Mattei et al. (2014), the Ashin (-Nain) to Baft oceanic crust spreading may have started in the Late Triassic to Early Jurassic in an ocean-continent transition zone (OCTZ) spreading system situated between the Sanandaj-Sirjan Zone and Central-East Iranian Microcontinent (Fig. 9a). This was followed by mid-Cretaceous (~ 107 Ma; Fig. 9b) subduction initiation. Based on the age of radiolarian cherts, if extension related to subduction initiation in the Ashin area occurred at ~ 107-94 Ma (~ 13 Myr long episode) at a supposed convergence and sinking average rate of 10 cm/yr (e.g., van der Meer et al., 2018), then the subducting oceanic crust had a width of ~ 1300 km. Such an oceanic basin could have formed by a spreading rate of ~ 1.4 cm/yr during transition from an ocean-continent transition zone (OCTZ) spreading system (in ~ 200 Ma: Late Triassic to Early Jurassic) to a subduction initiation (in ~ 107 Ma) (Fig. 9a). This means the presence of an old and cold subducting oceanic slab (~ 90 Myrs) in the subduction initiation of Ashin forearc ophiolite, and which is ascribed to lack of Nb-enriched slab melts by Yu et al. (2022).

During slab sinking and asthenospheric mantle upwelling, a proto-forearc crust was generated between the sinking slab and the continental margin (Fig. 9b). Before 107 Ma, the first forearc oceanic crust and related pillow lavas were produced by upwelling the depleted mantle melts with no chemical interaction with Neo-Tethyan subducted slab-derived fluids. The fluid contribution from the sinking slab to depleted MORB-type mantle (DMM) asthenosphere would have been minor during the earliest subduction initiation (Whattam and Stern, 2011).

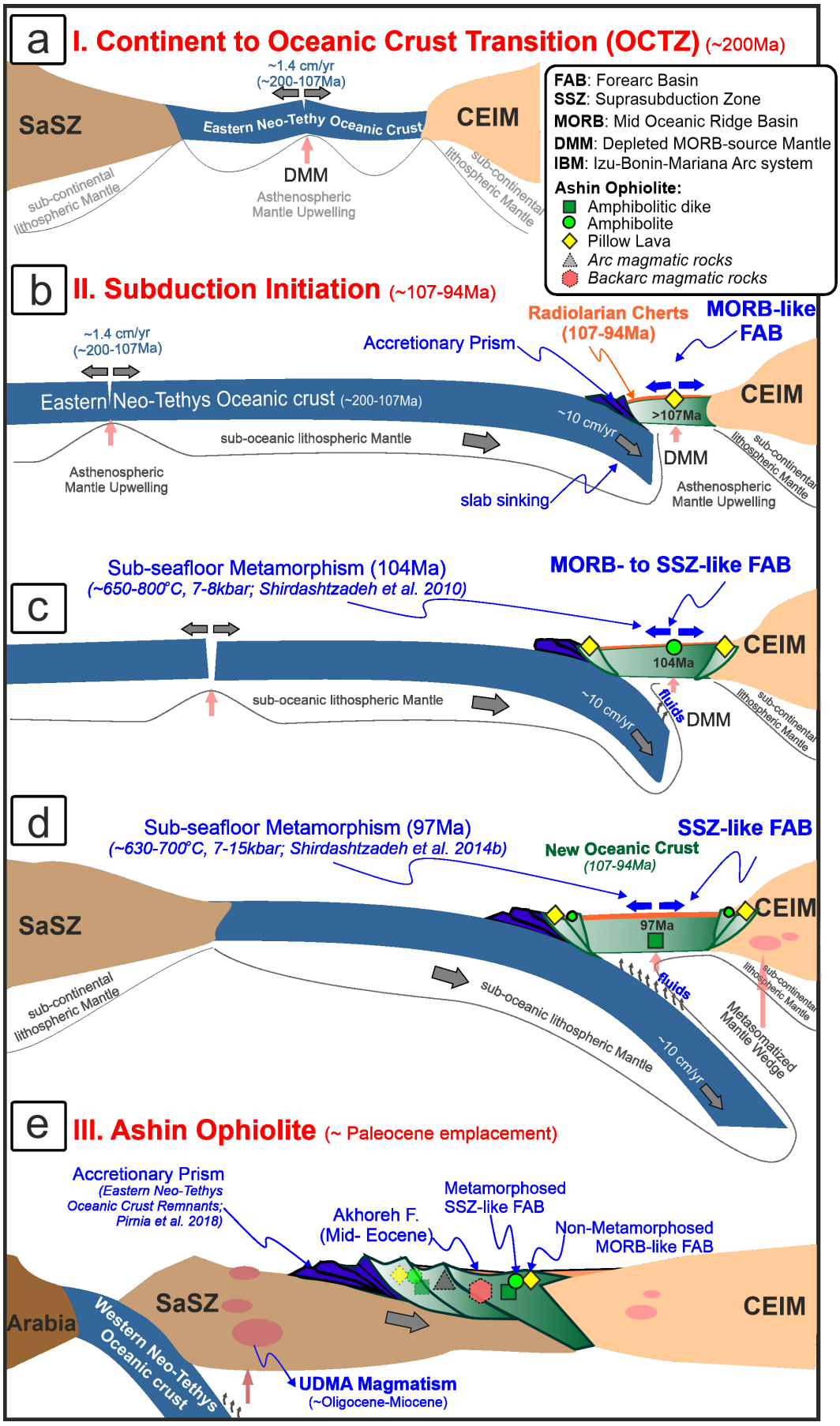

Fig. 9 - Schematic model (not to scale) for Neo-Tethyan Forearc basin of Ashin ophiolite (geological events from 97 Ma to Paleocene are not shown and discussed). CEIM= Central-East Iranian Microcontinent; SaSz = Sanandaj-Sirjan Zone; UDMA = Urumieh-Dokhtar magmatic arc.

Thus, the forearc basin grew as evidenced by the descending ages of pillow lavas (~ 107 Ma), amphibolites (~ 104 Ma), and amphibolitic dikes (~ 97 Ma), as well as their melt enrichment from MORB-like FAB (pillow lavas and amphibolites) to SSZ-like FAB (amphibolitic dikes) by increasing fluid contribution from the sinking slab to DMM asthenosphere (Fig. 9b-d).

If the forearc zone in the Ashin area occurred at ~ 107-94 Ma (~ 13 Myrs; based on radiolarian fauna ages by Shirdashtzadeh et al., 2015) at a supposed spreading rate similar to Neo-Tethys oceanic basin (~1.4 cm/yr; Fig. 9a), then the new forearc oceanic crust might have reached to ~ 180 km wide (Fig. 9d). By progressive closure of this forearc oceanic basin, it expected that arc magmatism and consequently backarc magmatism might have occurred from 97 Ma to Paleocene (Fig. 9e), similar to Nain ophiolite (Shirdashtzadeh et al., 2014a), Khoy-Maku of NW Iran (Moghadam et al., 2019a), Torbat-e-Heydarieh ophiolite of NE Iran (Moghadam et al., 2019b), and towards the west on the Bitlis-Zagros Suture Zone for the Late Cretaceous (Cenomanian-Campanian) development of an intra-oceanic arc-back arc system within the closing southern branch of Neo-Tethys Ocean (Ural et al., 2015; 2022).

Occurrence of backarc basin and boninitic melts has also documented in Nain ophiolitic mélange (i.e., Cr# of spinels and the calculated Al_2O_3 and FeO^t/MgO ratio for the parental melts of the chromitite patches; Ghazi et al., 2010) However, investigation of backarc basin rocks and further events is beyond the scope of this research work.

Finally, the oceanic basin closure and emplacement time was in the Paleocene based on middle Eocene Akhoreh Formation that covered this ophiolite (Mallah, 2021). Thus, the forearc basin oceanic crust was short-lived (~ 13 Myrs) in comparison with the basin in which subducting eastern Neo-Tethyan oceanic crust was formed (~ 90 Myrs) before subduction. Meanwhile, the new forearc oceanic plates could have been accreted on the subducting slab in the trench zone and on the continental crust (Fig. 9b-d). Based on field observations and geochemistry, the protolith of Ashin amphibolitic dikes intruded the lithospheric forearc mantle in the lower portion of the oceanic lithosphere (Fig. 1S-d) and above a metasomatized mantle wedge. The high-grade sub-seafloor metamorphism of the Ashin (and also Nain, and Dehshir; Fig. 8) amphibolites and amphibolitic dikes at early 104 Ma and 97 Ma could be related to formation in a relatively more developed forearc subduction system with progressive hydrothermal fluid circulation and upwelling the asthenospheric mantle heat flows. Finally, accretionary orogenic and collisional episodes resulted in formation of discrete ophiolitic mélanges from Ashin to Nain, Dehshir, and Baft (Fig. 9e).

CONCLUDING REMARKS

In the northern Nain-Baft ophiolitic belt, basaltic magmas clearly differ from typical N-MORB magmas by higher LILE (and LREE) but lower Nb, Ta contents than the N-MORB. The geochemical signatures (e.g., $Sm/Nd > 0.4$, $Lu/Hf > 0.3$, $Ce_N/Yb_N < 1.2$, $Dy_N/Yb_N < 1.2$, $Gd_N/Yb_N < 1$, $La_N/Yb_N < 1$, $Th/Nb < 0.2$, $\varepsilon Nd_I > 9$) of amphibolite and pillow lavas of the Ashin ophiolite are consistent with forearc (FAB) magmatism in a Late Cretaceous subduction initiation setting. Because the pillow lavas (age of overlying radiolarian cherts: ~ 107-94 Ma) have been formed in a low-temperature MORB-like forearc setting, they are affected by greenschist facies metamorphism.

Previous geochronological (radiolarian cherts overlying the pillow lavas: ~ 107Ma) and our new geochemical signatures (e.g., low HFSE, LILE and HREE values of whole rock, and the negative Eu anomaly of clinopyroxene ($Eu/Eu^*_{CPX} < 1$) crystallized after plagioclase) for the Ashin ophiolite pillow lavas support a FAB setting during subduction initiation in late Late Cretaceous from 107 to 97 Ma.

The geochronological (metamorphic zircon U-Pb age: 104 Ma) and geochemical features (e.g., high HFSE, LILE and HREE values of whole rock, and the positive Eu anomaly of clinopyroxene ($Eu/Eu^*_{CPX} > 1$) crystallized before plagioclase) of Ashin ortho-amphibolites support a MORB-like to SSZ-like FAB setting occurred at ~ 04 Ma. The metamorphism of the amphibolites (magmatic zircon U-Pb age: ~ 104 Ma) and then amphibolitic dikes (magmatic zircon U-Pb age: ~ 97 Ma) could have occurred owing to the progressive development of Ashin subduction zone initiation and maturation in Cretaceous, not by heating during Paleocene continental collision orogeny.

ACKNOWLEDGMENTS

The authors acknowledge the University of Isfahan (Iran), the University of Texas at Austin (USA), the University of Brasilia (Brazil), and Montanuniversität Leoben (Austria) for providing scientific and technical assistance for chemical analyses. The authors are grateful to Professor Chris Harris, Fernando Corfu, and Robert J. Stern for their constructive feedback on the earlier version of manuscript. The authors appreciate encouragement and constructive comments by Professors Y. Dilek, K. Sayit, and G. Borghini that greatly helped to improve this paper.

REFERENCES

Agard P., Omrani J., Jolivet L., Whitechurch H., Vrielynck B., Spakman W., Monié P., Meyer B. and Wortel R., 2011. Zagros orogeny: A subduction-dominated process. Geol. Mag., 148: 692-725. https://doi.org/10.1017/S001675681100046X.

Allen P.A. and Allen J.R., 1990. Basin analysis: Principles and applications. Blackwell Sci. Publ., Oxford, 451 pp.

Alparslan G. and Dilek Y., 2018. Seafloor spreading structure, geochronology, and tectonic evolution of the Küre ophiolite, Turkey: a Jurassic continental backarc basin oceanic lithosphere in southern Eurasia. Lithosphere, 10 (1): 14-34. https://doi.org/10.1130/L641.1.

Azizi H. and Moinevaziri H., 2009. Review of the tectonic setting of Cretaceous to Quaternary volcanism in northwestern Iran. J. Geodyn., 47: 167-179. https://doi.org/10.1016/j.jog.2008.12.002.

Balci U. and Sayit K., 2020. Diabase dykes from Boğazkale (Çorum), Central Anatolia: Geochemical insights into the geodynamical evolution of the northern branch of Neotethys. Geochemistry, 80 (2), 125602. https://doi.org/10.1016/j.chemer.2020.125602.

Becker T.W. and Faccenna C., 2011. Mantle conveyor beneath the Tethyan collisional belt. Earth Planet. Sci. Lett., 310: 453-461. https://doi.org/10.1016/j.epsl.2011.08.021.

Berberian F. and Berberian M., 1981. Tectono-plutonic episodes in Iran. In: H.K. Gupta and F.M. Delany (Eds.). Zagros Hindukush, Himalaya geodynamic evolution, Am. Geophys. Union, p. 5-32. https://doi.org/10.1029/95EO00198.

Bortolotti V., Chiari M., Göncüoglu M.C., Principi G., Saccani E., Tekin U.K. and Tassinari R., 2018. The Jurassic-Early Cretaceous basalt-chert association in the ophiolites of the Ankara Mélange, east of Ankara, Turkey: age and geochemistry. Geol. Mag., 155 (2): 451-478. https://doi.org/10.1017/S0016756817000401

Choi S., Mukasa S. and Shervais J., 2008. Initiation of Franciscan subduction along a large-offset fracture zone: Evidence from mantle peridotites, Stonyford, California. Geol., 36 (8): 595-598.

Corfu F., Hanchar J.M., Hoskin P.W.O. and Kinny P., 2003. Atlas of Zircon textures. Rev. Miner. Geochem., 53 (1): 469-500. https://doi.org/10.2113/0530469.

Cox K., Bell J. and Pankhurst R., 1979. The Interpretation of igneous rocks. London, Allen and Unwin, 450 pp.

DePaolo D.J. and Wasserburg G.J., 1979. Petrogenetic mixing models and Nd-Sr isotopic patterns. Geochim. Cosmochim. Acta, 43: 615-627.

Dilek Y. and Furnes H., 2009. Structure and geochemistry of Tethyan ophiolites and their petrogenesis in subduction rollback systems. Lithos, 13: 1-20. https://doi.org/10.1016/j.lithos.2009.04.022.

Dilek Y. and Furnes H., 2011. Ophiolite genesis and global tectonics: Geochemical and tectonic fingerprinting of ancient oceanic lithosphere. Geol. Soc. Am. Bull., 123(3/4): 387-411. https://doi.org/10.1130/B30446.1.

Dilek Y. and Furnes H., 2014. Ophiolites and their origins. Elements, 10: 93-100. https://doi.org/10.2113/gselements.10.2.93.

Dilek Y. and Furnes H., 2019. Tethyan ophiolites and Tethyan seaways. J. Geol. Soc., 176: 899-912. https://doi.org/10.1144/jgs2019-129.

Dilek Y. and Thy P., 2009. Island arc tholeiite to boninitic melt evolution of the Cretaceous Kizildag (Turkey) ophiolite: Model for multi-stage early arc-forearc magmatism in Tethyan subduction factories. Lithos, 113: 68-87. https://doi.org/10.1016/j.lithos.2009.05.044.

Fergusson C.L., Nutman A.P., Mohajjel M. and Bennett V.C., 2016. The Sanandaj - Sirjan Zone in the Neo-Tethyan suture, western Iran: Zircon U - Pb evidence of late Palaeozoic rifting of northern Gondwana and mid-Jurassic orogenesis. Gondw. Res., 40: 43-57. https://doi.org/10.1016/j.gr.2016.08.006.

Furnes H. and Dilek Y., 2017. Geochemical characterization and petrogenesis of intermediate to silicic rocks in ophiolites: A global synthesis. Earth-Sci. Rev., 166: 1-37.

Furnes H. and Dilek Y., 2022. Archean versus Phanerozoic oceanic crust formation and tectonics: Ophiolites through time. Geosyst. Geoenviron., 1 (1): 100004. https://doi.org/10.1016/j.geogeo.2021.09.004

Furnes H., de Wit M. and Dilek Y., 2014. Four billion years of ophiolites reveal secular trends in oceanic crust formation. Geosci. Front., 5 (4): 571-603. https://doi.org/10.1016/j.gsf.2014.02.002.

Furnes H., Dilek Y. Zhao G., Safonova I. and Santosh M., 2020. Geochemical characterization of ophiolites in the Alpine-Himalayan Orogenic Belt: Magmatically and tectonically diverse evolution of the Mesozoic Neotethyan oceanic crust. Earth-Sci. Rev., 208: 103258. https://doi.org/10.1016/j.earscirev.2020.103258.

Garrels R. and Mackenzie F., 1971. Evolution of sedimentary rocks. W.W. Norton and Co. Int., New York, 394 pp.

Ghazi A. and Hassanipak A., 2000. Petrology and geochemistry of the Shahr-Babak ophiolite, Central Iran. Geol. Soc. Am. Spec. Pap., 349: 485-497. https://doi.org/10.1130/0-8137-2349-3.485.

Ghazi J. M., Moazzen M., Rahghoshay, M. and Moghadam, H. S., 2011. The geodynamic setting of the Nain ophiolites; Central Iran: Evidence from chromian spinels in the chromitites and associated rocks. Ofioliti, 36(1), 59-76. https://doi.org/10.4454/ofioliti.v36i1.394

Goes S., Agrusta R., van Hunen J. and Garel F., 2017. Subduction-transition zone interaction: A review. Geosphere, 13: 644-664. https://doi.org/10.1130/GES01476.1

Hassanipak A. and Ghazi A., 2000. Petrochemistry, ^{40}Ar-^{39}Ar ages and tectonics of the Naein ophiolite, Central Iran. GSA Ann. Meet., p. 237-238.

Hebert R. and Laurent R., 1990. Mineral chemistry of the plutonic section of the Troodos Ophiolite: new constraints for genesis of arc-related ophiolites. Proceed. Symp. "Troodos 1987", Geol. Surv. Dept., Cyprus.

Hekinian R.B.T., 1982. Ocean Floor Metamorphism. Chapter 9. Oceanogr. Ser., Elsevie, p. 265-290. https://doi.org/10.1016/S0422-9894(08)70951-6.

Hu J., Jiang N., Fan W. and Zhang S., 2017. Comparison of metamorphic zircons from granulite xenoliths and granulite terrain in northern North China Craton. Precambrian Res., 303: 414-427. https://doi.org/10.1016/j.precamres.2017.05.019.

Hyndman R.D., 2019. Origin of regional Barrovian metamorphism in hot backarcs prior to orogeny deformation. Geochem. Geophys. Geosyst., 20: 460-469. https://doi.org/10.1029/2018GC007650.

Kananian A., Juteau T., Bellon H., Darvishzadeh A. and Sabzehi M., 2001. The ophiolite massif of Kahnuj (western Makran, southern Iran): new geological and geochronological data. C.R. Acad. Sci., Ser. 2, Earth Planet. Sci., 332: 543-552. https://doi.org/10.1016/S1251-8050(01)01574-9.

Kelemen B., Hanghøj K. and Greene A.R., 2007. One view of the geochemistry of subduction-related magmatic arcs, with an emphasis on primitive andesite and lower crust. In: H. Holland, and K. Turekian (Eds.). Treatise on geochemistry, Pergamon, Oxford, p. 1-70. https://doi.org/10.1016/B0-08-043751-6/03035-8.

Khedr M., Arai S., Python M. and Tamura A., 2014. Chemical variations of abyssal peridotites in the central Oman ophiolite: evidence of oceanic mantle heterogeneity. Gondw. Res., 25: 1242-1262.

Kojima S., Naka T., Kimura K., Mengal J., Siddiqui R. and Bakht M., 1994. Mesozoic radiolarians from the Bagh Complex in the Muslim Bagh area, Pakistan: their significance in reconstructing the geologic history of ophiolites along the Neo-Tethys suture zone. Bull. Geol. Surv Jpn., 45: 63-97.

Lu G., Kaus B.J.P., Zhao L. and Zheng T., 2015. Self-consistent subduction initiation induced by mantle flow. Terra Nova 27 (2): 130-138. https://doi.org/10.1111/ter.12140.

Malahoff A., Feden R.H. and Fleming H.S., 1982. Magnetic anomalies and tectonic fabric of marginal basins north of New Zealand. J. Geophys. Res., 87: 4109-4125.

Mallah M., 2021. Depositional environment, diagenesis and tectonic setting of the clastic rocks of lower part of the Akhoreh Formation (Eocene), Shurab section, north of Naein. MSc Thesis, Univ. Isfahan, Isfahan, Iran, 115 pp.

Martinez F. and Taylor B., 2002. Mantle wedge control on back-arc crustal accretion. Nature, 416: 417-420.

Mattei M., Cifelli F., Muttoni G. and Rashid H., 2014. Post-Cimmerian (Jurassic - Cenozoic) paleogeography and vertical axis tectonic rotations of Central Iran and the Alborz Mountains. J. Asian Earth Sci., 102: 92-101. https://doi.org/10.1016/j.jseaes.2014.09.038.

Ghazi J. M., Moazzen M., Rahghoshay, M. and Moghadam, H. S., 2011. The geodynamic setting of the Nain ophiolites; Central Iran: Evidence from chromian spinels in the chromitites and associated rocks. Ofioliti, 36(1), 59-76. https://doi.org/10.4454/ofioliti.v36i1.394

Moghadam H.S. and Stern R.J., 2015. Ophiolites of Iran: Keys to understanding the tectonic evolution of SW Asia: (II) Mesozoic ophiolites. J. Asian Earth Sci., 100: 31-59. https://doi.org/10.1016/j.jseaes.2014.12.016.

Moghadam H.S. and Stern R.J., 2021. Subduction initiation causes broad upper plate extension: The Late Cretaceous Iran example. Lithos, 398-399: 106296

Moghadam H.S., Corfu F., Stern R.J. and Lotfi Bakhsh A., 2019a. The Eastern Khoy metamorphic complex of NW Iran: a Jurassic ophiolite or continuation of the Sanandaj-Sirjan Zone? J. Geol. Soc., London, 176: 517-529. https://doi.org/10.1144/jgs2018-081

Moghadam H.S., Stern R.J., Griffin W.L., Khedr M.Z., Kirchenbaur M., Ottley C.J., Whattam S.A., Kimura J.-I., Ghorbani G., Gain S., O'Reilly S.Y. and Tamura A., 2019b. Subduction initiation and back-arc opening north of Neo-Tethys: Evidence from the Late Cretaceous Torbat-e-Heydarieh ophiolite of NE Iran. GSA Bull., 132: 1083-1105. https://doi.org/10.1130/B35065.1.

Moghadam H.S., Whitechurch H., Rahgoshay M. and Monsef I., 2009. Significance of Nain-Baft ophiolitic belt (Iran): Short-lived, transtensional Cretaceous backarc oceanic basins over the Tethyan subduction zone. C.R. Geosci., 341 (12): 1016-1028. https://doi.org/10.1016/j.crte.2009.06.011.

Molnar P. and Atwater T., 1978. Interarc spreading and Cordilleran tectonics as alternates related to the age of subducted oceanic lithosphere. Earth Planet. Sci. Lett., 41: 330-340. https://doi.org/10.1016/0012-821X(78)90187-5.

Omrani H., Moazzen M., Oberhänsli R., Altenberger U. and Lange M., 2013. The Sabzevar blueschists of the North-Central Iranian micro-continent as remnants of the Neotethys related oceanic crust subduction. Int. J. Earth Sci., 102: 1491-1512.

Pearce J.A., 2014. Ophiolites: immobile elements fingerprinting of ophiolites. Elements, 10 (2): 101-108.

Pearce J.A., Stern R.J., Bloomer S.H. and Fryer P., 2005. Geochemical mapping of the Mariana arc-basin system: Implications for the nature and distribution of subduction components. Geochem. Geophys. Geosyst., 6 (7). https://doi.org/10.1029/2004GC000895.

Pedersen R., Searle M.P. and Corfield R.I., 2001. U-Pb zircon ages from the Spontang Ophiolite, Ladakh Himalaya. J. Geol. Soc. London, 158: 513-520.

Pirnia T., Saccani E. and Arai S., 2018. Spinel and plagioclase peridotites of the Nain ophiolite (Central Iran): Evidence for the incipient stage of oceanic basin formation. Lithos, 310-311: 1-19. https://doi.org/10.1016/j.lithos.2018.04.001.

Pirnia T., Saccani E., Torabi G., Chiari M., Spela G. and Barbero E., 2020. Cretaceous tectonic evolution of the Neo-Tethys in Central Iran: Evidence from petrology and age of the Nain-Ashin ophiolitic basalts. Geosci. Front., 11 (1): 57-81. https://doi.org/10.1016/j.gsf.2019.02.008.

Reagan M.K., Ishizuka O., Stern R.J., Kelley K.A., Ohara Y., Blichert-Toft J., Bloomer S.H., Cash J., Fryer P., Hanan B.B. and Hickey-Vargas R., 2010. Fore-arc basalts and subduction initiation in the Izu-Bonin-Mariana system. Geochem. Geophys. Geosyst., 11. https://doi.org/10.1029/2009GC002871.

Rolland Y., Galoyan G., Sosson M., Melkonyan R. and Avagyan A., 2010. The Armenian Ophiolite: insights for Jurassic back-arc formation, Lower Cretaceous hot spot magmatism and Upper Cretaceous obduction over the South Armenian Block. In: M. Sosson, N. Kaymakci, R.A. Stephenson, F. Bergerat and V. Starostenko (Eds.), Sedimentary basin tectonics from the Black Sea and Caucasus to the Arabian Platform. Geol. Soc. London, 340: 353-382. https://doi.org/10.1144/SP340.15

Rubatto D., 2017. Zircon: The Metamorphic

Saccani E., 2015. A new method of discriminating different types of post-Archean ophiolitic basalts and their tectonic significance using Th-Nb and Ce-Dy-Yb systematics. Geosci. Front., 6 (4): 481-501. https://doi.org/10.1016/j.gsf.2014.03.006.

Sdrolias M. and Müller R.D., 2006. Controls on back-arc basin formation. Geochem. Geophys. Geosyst., 7. https://doi.org/10.1029/2005GC001090.

Sharkovski M., Susov M. and Krivyakin B., 1984. Geology of the Anarak area (Central Iran), Explanatory text of the Anarak quadrangle map, 1:250,000: V/O Technoexport Rep. 19, Geol. Surv. Iran, 143 pp.

Shervais J.W., 1982. Ti-V plots and the petrogenesis of modern and ophiolitic lavas. Earth Planet. Sci. Lett., 59: 101118. https://doi.org/10.1016/0012-821X(82)90120-0.

Shervais J.W., Reagan M.K., Godard M., Prytulak J., Ryan J.G., Pearce J.A., et. al., 2021. Magmatic response to subduction initiation, Part II: Boninites and related rocks of the Izu-Bonin Arc from IODP Expedition 352. Geochem. Geophys. Geosyst. 22: e2020GC009093. https://doi.org/10.1029/2020GC009093

Shervais J.W., Reagan M.K., Haugen E., Almeev R.R., Pearce J.A., Prytulak J., et al., 2019. Magmatic response to subduction initiation: Part 1. Fore-arc basalts of the Izu-Bonin arc from IODP Expedition 352. Geochem. Geophys. Geosyst., 20: 314-338. https://doi.org/10.1029/2018GC007731.

Shirdashtzadeh N., Kachovich S., Aitchison J.C. and Samadi R., 2015. Mid-Cretaceous radiolarian faunas from the Ashin Ophiolite (western Central-East Iranian Microcontinent). Cretac. Res., 56: 110-118. https://doi.org/10.1016/j.cretres.2015.04.003.

Shirdashtzadeh N., Torabi G. and Arai S., 2010. Metamorphism and metasomatism in the Jurassic Nain ophiolitic mélange, Central Iran. N. Jahrb. Geol. Paläont., Abh., 255 (3): 255-275. https://doi.org/10.1127/0077-7749/2009/0017.

Shirdashtzadeh N., Torabi G. and Arai S., 2011. Two Mesozoic oceanic phases recorded in the basic and metabasic rocks of the Nain and Ashin-Zavar ophiolitic mélanges (Isfahan province, Central Iran). Ofioliti, 36 (2): 191-205.

Shirdashtzadeh N., Torabi G. and Morishita T., 2020. Evolution of lithospheric mantle in the north of Nain-Baft oceanic crust (Neo-Tethyan ophiolite of Ashin, Central Iran). Isl. Arc, 29: 1-12. https://doi.org/10.1111/iar.12342.

Shirdashtzadeh N., Torabi G. and Samadi R., 2014a. Geochemistry of pillow lavas and their clinopyroxene: ophiolitic mélanges of Nain and Ashin, northeastern Isfahan province. J. Econ. Geol., 6 (1): 49-70. https://doi.org/10.22067/econg.v6i1.19911.

Shirdashtzadeh N., Torabi G., Meisel T., Arai S., Bokhari S., Samadi R. and Gazel E., 2014b. Origin and evolution of metamorphosed mantle peridotites of Darreh Deh (Nain Ophiolite, Central Iran): Implications for the Eastern Neo-Tethys evolution. 273 (1): 89-120. https://doi.org/10.1127/0077-7749/2014/0418.

Stampfli G.M. and Borel G.D., 2002. A plate tectonic model for the Paleozoic and Mesozoic constrained by dynamic plate boundaries and restored synthetic oceanic isochrones. Earth Planet. Sci. Lett., 196: 17-33. https://doi.org/10.1016/S0012-821X(01)00588-X.

Stern R.J. and Gerya T., 2018. Subduction initiation in nature and models: A review. Tectonophysics, 746: 173-198. https://doi.org/10.1016/j.tecto.2017.10.014.

Stern R.J., Moghadam H.S., Pirouz M. and Mooney W., 2021. The geodynamic evolution of Iran. Ann. Rev. Earth Planet. Sci., 49: 9-36.

Stern R.J., Reagan M., Ishizuka O., Ohara Y. and Whattam S., 2012. To understand subduction initiation, study forearc crust: To understand forearc crust, study ophiolites. Lithosphere, 4 (6): 469-483. https://doi.org/10.1130/L183.1

Sun S.S. and McDonough W.F., 1989. Chemical and isotopic systematics of oceanic basalts: Implications for mantle composition and processes. Geol. Soc. London Spec. Publ., 42 (1): 313-345. https://doi.org/10.1144/GSL.SP.1989.042.01.19.

Topuz G., Çelik Ö.F., Şengör A.M.C., Altintaş I.E., Zack T., Rolland Y. and Barth M., 2013. Jurassic ophiolite formation and emplacement as backstop to a subduction-accretion complex in northeast Turkey, the refahiye ophiolite, and relation to the Balkan ophiolites. Am. J. Sci., 313 (10): 1054–-1087. https://doi.org/10.2475/10.2013.04

Torabi G., Shirdashtzadeh N., Arai S. and Koepke J., 2011. Paleozoic and Mesozoic ophiolites of Central Iran: amphibolites from Jandaq, Posht-e-Badam, Nain and Ashin ophiolites. N. Jahrb. Geol. Paläont., Abh., 262 (3): 227-240. https://doi.org/10.1127/0077-7749/2011/0194.

Ural M., Arslan M., Göncüoğlu M.C., Tekin U.K. and Kürüm S., 2015. Late Cretaceous arc and back-arc formation within the Southern Neotethys: whole-rock, trace element and Sr-Nd-Pb isotopic data from basaltic rocks of the Yüksekova Complex (Malatya-Elazığ, SE Turkey). Ofioliti, 40 (1): 53-72.

Ural M., Sayit K. and Tekin U.K., 2022. Whole-rock and Nd-Pb isotope geochemistry and radiolarian ages of the volcanics from the Yüksekova complex (Maden area, Elazığ, E Turkey): implications for a Late Cretaceous (Santonian-Campanian) back-arc basin in the Southern Neotethys. Ofioliti, 47 1): 65-83.

van der Meer D.G., van Hinsbergen D.J.J. and Spakman W., 2018. Atlas of the underworld: Slab remnants in the mantle, their sinking history, and a new outlook on lower mantle viscosity. Tectonophysics, 723: 309-448. https://doi.org/10.1016/j.tecto.2017.10.004

Van Horne A., Sato H. and Ishiyama T., 2017. Evolution of the Sea of Japan back-arc and some unsolved issues. Tectonophysics, 710-711: 6-20. https://doi.org/10.1016/j.tecto.2016.08.020.

Whattam S.A. and Stern R.J., 2011. The 'subduction initiation rule': a key for linking ophiolites, intra-oceanic forearcs, and subduction initiation. Contrib. Miner. Petrol., 162: 1031-1045. https://doi.org/10.1007/s00410-011-0638-z.

Wilmsen M., Fürsich F. and Majidifard M., 2015. An overview of the Cretaceous stratigraphy and facies development of the Yazd Block, western Central Iran. J. Asian Earth Sci., 102: 73-91. https://doi.org/10.1016/j.jseaes.2014.07.015.

Winchester J. and Floyd P., 1977. Geochemical discrimination of different magma series and their differentiation products using immobile elements. Chem. Geol., 20: 325-343.

Winchester J.A., Max M.D. and Long C.B., 1987. Trace Element geochemical correlation in the Reworked Proterozoic Dalradian Metavolcanic Suites of the Western Ox Mountains and NW Mayo Inliers, Ireland. Geol. Soc. London Spec. Publ., 33: 489-502. https://doi.org/10.1144/GSL.SP.1987.033.01.33.

Xia L. and Li X., 2019. Basalt geochemistry as a diagnostic indicator of tectonic setting. Gondw. Res., 65: 43-67. https://doi.org/10.1016/j.gr.2018.08.006.

Yamasaki T., Maeda J. and Mizuta T., 2006. Geochemical evidence in clinopyroxenes from gabbroic sequence for two distinct magmatisms in the Oman ophiolite. Earth Planet. Sci. Lett., 251: 52-65. https://doi.org/10.1016/j.epsl.2006.08.027.

Yatheesh V., Aswini K.K., Kamesh Raju K.A., John Savio J., Gawas A. and Dewangan P., 2021. Morphotectonic signatures and revised timing of opening of the Andaman Backarc Basin, Northeast Indian Ocean. Tectonophysics, 820: 229108. https://doi.org/10.1016/j.tecto.2021.229108.

Yeganehfar H., Ghorbani M.R., Shinjo R. and Ghaderi M., 2013. Magmatic and geodynamic evolution of Urumieh-Dokhtar basic volcanism, Central Iran: major, trace element, isotopic, and geochronologic implications. Int. Geol. Rev., 55: 767-786.

Yu M., Yumul G.P., Dilek Y., Yan Y. and Huang C.Y., 2022. Diking of various slab melts beneath forearc spreading center and age constraints of the subducted slab. Earth Planet. Sci. Let., 579: 117367. https://doi.org/10.1016/j.epsl.2022.117367

Zheira G., Masoudi F. and Rahimzadeh B., 2020. Geochemical constraints on Eocene-Miocene geodynamic and magmatic evolution of the Varan-Naragh area, Urumieh-Dokhtar Magmatic Arc, Iran. Can. J. Earth Sci., 57 (9): 1048-1065. https://doi.org/10.1139/cjes-2019-0129.

Zheng Y., 2019. Subduction zone geochemistry: Geosci. Front., 10 (4): 1223-1254. https://doi.org/10.1016/j.gsf.2019.02.003.

Zhong L.F., Xia B., Zhang Y., Wang R., Wei D. and Yang Z., 2006. SHRIMP Age determination of the diabase in Luobusa Ophiolite, Southern Xizang (Tibet). Geol. Rev., 52 (2): 224-229.

Received, March 6, 2022
Accepted, June 22, 2022